

Final Project Report:

Alloy Development and Characterization Services
(for United States Currency Applications)

Interagency Agreement #1404-642-01

Between:

The United States Mint,
U.S. Department of Treasury

AND

The National Institute of Standards and Technology,
U.S. Department of Commerce

Prepared by:

Eric A. Lass¹, Mark R. Stoudt¹, Tony Ying², and Carelyn E. Campbell¹

¹*Materials Science & Engineering Division,
Material Measurement Laboratory,
National Institute Standards and Technology,
U.S. Department of Commerce*

²*The United States Mint,
U.S. Department of Treasury*

Executive Summary

Due to the rising cost of materials, the US Mint is seeking alternative coinage alloys to reduce the production cost for US nickels, dimes, and quarters. Commercial C71300¹, a 0.75 copper, 0.25 nickel by mass cupronickel alloy (in shorthand form Cu-25Ni) is currently used for the 5-cent coin and as a cladding material for the 10-cent and 25-cent coins. The present cost to produce a 5-cent coin is approximately 7.5 cents. In response, Congress has tasked the US Mint to reduce the cost to produce the 5, 10, and 25-cent coins between (25 to 40) percent without changing its current processing and production capabilities. As part of this effort, the US Mint and the National Institute of Standards and Technology (NIST) Materials Science and Engineering Division (MSED) established an Interagency Agreement (IA) in June 2014 to develop a series of new, lower-cost coinage alloys. These new alloys are based on current nickel-silver alloys (also referred to as German-silver), which consist of copper, nickel, and zinc. Specifically, NIST agreed to develop three prototype alloys to replace the current coinage materials. The prototypes were:

1. An alloy based on C77000, a nickel-silver based alloy with a nominal composition of Cu-0.18Ni-0.27Zn mass fraction. This alloy is the first-step in the cost reduction strategy with an anticipated reduction in the production cost of the monolithic 5-cent coin of approximately 22 %.
2. An alloy based on commercial C99750, an alloy comprised primarily of Cu, Ni, Zn, and Mn. Because it has a higher Zn content than C77000, this alloy could further reduce the production cost of the 5-cent coin to realize a total reduction of approximately 40 percent over the original cost.
3. An alloy based on a second modification of commercial C99750 that will be used as a cladding material for the 10-cent and 25-cent coins.

The modified C77000 and the C99750 are to be seamless replacements for the C71300 alloy currently used in the 5-cent coin. In this context, a seamless replacement means that no changes to any current coin manufacturing operations or usage applications will be needed to accommodate the new coinage alloy. To be considered a viable prototype, the replacement must exhibit several specific characteristics. The most important of these is the electrical conductivity, which enables a coin to be used in most vending machine and coin sorting technologies. Therefore, the conductivity of a replacement alloy must closely match to the conductivity of the C71300. The mechanical properties of a replacement alloy must be similar to those of the current alloy so that the current stamping processes do not need to be altered to produce a coin. Good corrosion resistance and wear properties are also needed to maintain color stability and to ensure long lifetimes in circulation. Esthetic factors, such as the alloy color (i.e.

¹ Note all references to commercial alloys and products are provided to enable clear understanding of the work presented. Such identification does not imply recommendation or endorsement by the National Institute of Standards and Technology, nor does it imply that the alloys or products identified are necessarily the best available for the purpose.

it must maintain a silver appearance) and the relative mass of a test coin, are also to be considered to minimize the change to the general public.

An Integrated Computational Materials Engineering (ICME) materials design approach was adopted to develop the compositions of the replacement alloys. This included developing a series of CALPHAD-based models to describe the relevant properties of an alloy as a function of composition. These models included descriptions of electrical conductivity, color, and cost. The models were combined with a set of empirical models that were based on prior knowledge to establish the compositions of the new alloys. The prototypes were then physically characterized to determine how well each prototype met the design goals. If the design goals were not achieved, the models were refined based on the experimental results.

Design of Modified C77000

The first alloy designed was the modified C77000. Experimental characterization of commercial C77000 revealed that the relevant properties were sufficient to produce seamless replacement of C71300, with the exception of the electrical conductivity. Consequently, meeting the electrical conductivity property design requirements was the top design priority. The Mn composition dependence was the critical component in the electrical conductivity model. A small amount of Mn (0.03% mass fraction) is present in the commercial C77000 alloy and it is known to have a significant influence on the conductivity of the alloy. A second design priority was the controlling the atomic-level ordering that occurs when cooling from evaluated temperatures during processing. Since ordering strongly affects the conductivity and mechanical properties of the alloy, the designed alloy must avoid the natural formation of ordered phases during the current manufacturing processes, which include water quenching from elevated temperatures.

The electrical conductivity of C77000 is about 5.5 % to 5.7 % IACS (International Annealed Copper Standard), whereas that of C71300 is 5.45 % IACS. Using the composition-dependent conductivity model developed at the outset of the project, it was determined that replacing 1 % Zn with Ni would decrease the electrical conductivity by approximately 0.2 % IACS. The resulting alloys, named NIST C77D, exhibited a conductivity matching that of C71300; in addition it met all the other properties outlined by the US Mint. The conductivity model was then implemented to predict composition tolerance limits for each of the elements such that an alloy within these limits would be guaranteed to possess the appropriate conductivity, within a 0.2 % IACS margin of error set by the US Mint. Iron (Fe), an unavoidable impurity element in Cu-alloys, was also included in the composition tolerance determination. Two alloy compositions that were predicted to be on the extreme high and low ends of the conductivity limits were produced to test the calculated composition tolerances. It was determined that the predicted composition tolerances were sufficient to maintain a suitable range of electrical conductivity. A 20 % material cost savings is projected for the replacement of C71300 by NIST C77D'.

When the US Mint tested C77D in actual vending machine coin acceptors, the modification made to the coin thickness (necessary to offset the small density difference between C71300 and C77D so the coin weight remains unchanged) produced an electrical signature that slightly

differed from C71300 coins. This required a reduction in the target conductivity from 5.45 % to 5.35 % IACS, which was accommodated by a small increase to the Ni and Mn contents in the C77D composition. A provisional patent application has been filed for the resulting alloy, C77D' and a full patent application is currently in preparation.

Design of Modified C99750

Electrical conductivity, color and cost requirements were the primary design objectives for the development of a modified C99750 alloy. Commercial C99750 alloy contains up to 0.025 mass fraction lead, and up to 0.03 mass fraction aluminum. These elements are undesirable as they both have a large impact on the overall electrical conductivity. Lead is also an unwanted alloy addition due to potential health risks. Additional prototype compositions similar to C99750 are in this system, such as C99700 and C99710, but they also contain unwanted elements. Thus, no existing commercial alloy could serve as a basis for this design, and a limited amount of experimental data were available to calibrate the conductivity model in the composition region of interest. This required the design of additional model alloys to verify and improve the existing conductivity model.

Once the conductivity model was successfully adjusted for use in the C99-series, the first prototype composition designed for the 5-cent application matched all the design specifications outlined in the IA except for color. Unfortunately, the color of the material, which was found to be highly dependent on the measurement conditions, was determined to be too "yellow". A composition-based color model was then introduced to the design process to develop a new prototype composition. These new prototype alloys had a slight improvement in matching the desired color. However, the alloy color-property objective conflicts with the cost objectives for the C99. Improvement in color properties resulted in higher cost alloys compositions that were similar to already designed C77D alloy. The prototype alloy C99R represents the optimal composition for the two conflicting property objectives in the C99-series 5-cent application. Composition tolerances for the alloy were developed using the conductivity model and the experience gained from the development of C77D'. At the time of preparation of this report, the US Mint was in the process of characterizing the C99R alloy, and an invention disclosure was in preparation at NIST.

Design of the C99 Cladding Alloy

The primary design objectives for the C99-based cladding material were the cost, color, and mechanical properties. The conductivity design requirements were not as critical for the cladding used in the 10-cent and 25-cent coins as those used for the monolithic 5-cent coin. A lower target conductivity requirement, set initially at 2.0 % IACS, allows the cladding layer to be thicker than that needed using C71300, thereby reducing the thickness of the more expensive pure-Cu core in those coins. An initial prototype alloy, C99B, had an acceptable conductivity of 2.7 % IACS and was considered as the first potential candidate for the C99-series cladding alloys. However, the color and mechanical properties C99B required some adjustments. Fine-tuning the color and mechanical property models produced a new prototype, C99H, which was

then designed and characterized. The initial results of that characterization revealed that C99H demonstrated the desired conductivity, color, and mechanical properties. A larger heat of C99H was subsequently produced and provided to the US Mint for coin production and additional characterization. The US Mint is currently evaluating C99H as a potential cladding material.

One processing issue that occurred during the development of C99H was controlling the Mn-content in the alloy when casting. This resulted in Mn concentrations ranging from about 0.125 mass fraction to 0.14 mass fraction and corresponding electrical conductivities ranging from 2.8 % IACS to 2.6 % IACS, respectively. A composition variation of ± 0.2 % mass fraction is within the initial composition tolerance calculated by the conductivity model for a base conductivity of 2.8 % IACS. However, three separate Mn composition limits for the target conductivities of 2.6 ± 0.2 % IACS, 2.7 ± 0.2 % IACS, and 2.8 ± 0.2 % IACS have been provided in this report to ensure that the final alloy properties meet the expected specifications. The tolerances for the remaining elements are the same for each of the three specifications. An invention disclosure for C99H that includes the entire potential range in composition and conductivity was in preparation at the time of this report.

NIST employed a materials design approach centered on CALPHAD-based models to develop three new coinage materials for the US Mint to assuage the production cost of US coinage. The prototypes were designed using CALPHAD-base models for the thermodynamics, kinetics, electrical conductivity, and color. The computationally designed prototypes were produced and characterized in the NIST laboratories using processes as similar as possible to the actual manufacturing processes used by the US Mint.

All three prototype alloys are ready to be provided to US Mint material suppliers for up-scaling to commercial production levels. Some processing issues could arise during the transition to industrial levels that are not observed at the laboratory scale. (e.g., impurity concentrations in industrial quantities that are greater than those at the laboratory scale.) The computational design models should help address some of these issues. The patent protection process for each alloy is in progress and non-disclosure agreements are in place with two US Mint materials suppliers.

1. Introduction & Background

1.1. US Mint request to NIST

As the price of raw materials has increased, in particular copper (Cu) and nickel (Ni), the cost of producing US coinage currency has become increasingly prohibitive. As a result, the US Mint has developed a program looking at producing US coinage using lower cost materials [1]. Under this project, the US Mint approached NIST's Materials Science & Engineering Division (MSED) with the goal of designing a new metallic alloy to seamlessly replace the cupronickel (commercial alloy C71300) material presently used in the production of US 5-cent, 10-cent, 25-cent, and 50-cent denomination coins. A seamless replacement is defined such that the new material can be substituted for C71300 without any changes to current coin production processes; or cause any disruptions or required changes to commerce and commercial use of coinage, such as the banking and vending machine industries. As a starting point, the US Mint identified a currently available commercial alloy, C77000, which possesses nearly all the required properties for seamless integration (the only exception being the electrical conductivity). C77000 is an alloy comprised primarily of Cu, Ni, and zinc (Zn); and because it contains smaller amounts of Cu and Ni, replaced by the cheaper material Zn, the cost of C77000 is about 20 % less than C71300 in terms of required raw materials. The US Mint also proposed further reducing the material cost by substituting manganese (Mn) for Ni, creating an alloy with compositions similar to a number "specialty" commercial alloys designated C997x0 (where x equal to 0, 1, 2, 4, and 5 signifies different alloys), except that the properties of the new alloy would be tuned to again allow seamless substitution for C71300. Another alloy the US Mint proposed that NIST develop was a second alloy with similar composition to C997x0 except with lower conductivity for use as a cladding material in multilayer coins such as the dime and quarter. The US Mint proposed that NIST design a total of three new alloys:

- 1) A variant on commercial C77000, containing primarily Cu, Ni, and Zn, and
- 2) A lower-cost alloy containing Mn, both of which were to possess all the required properties for seamless replacement of C71300, and
- 3) A lower conductivity alloy also containing Mn for use as a cladding material.

1.2. Design requirements for seamless integration

The properties required of a material for seamless replacement of C71300 in US coinage applications, as outlined by the US Mint are:

Material Properties

- An electrical conductivity match to C71300, measured as $5.47 \% \pm 0.10 \%$ IACS (International Annealed Copper Standard) for coins presently in circulation, to within a $\pm 0.2 \%$ IACS tolerance.
- A white, silvery color, that when measured using the L, a^*, b^* color space, possesses an a^* (redness hue) of less than 2.5 and a b^* (yellowness) of less than 10.
- A yield strength of < 200 MPa, corresponding to a hardness value of < 80 HR15T or < 110 VHN.
- A tensile elongation to failure of $> 25 \%$.
- An initial working hardening coefficient comparable to C71300
- A wear resistance not greater than $5\times$ that of C71300.
- A corrosion resistance measured using a two-hour steam test ($100\text{ }^\circ\text{C}$, 100% relative humidity). After the two hours, the change in the b^* color vector must be < 11 for the bare metal, and < 5 with a protective coating applied to the surface.

Processing Constraints

- Annealing in air for 30 minutes at temperature between $650\text{ }^\circ\text{C}$ and $850\text{ }^\circ\text{C}$, followed by a water quench.

Microstructure Constraints

- A grain size less than $100\text{ }\mu\text{m}$ to ensure proper upsetting of the coins.

NIST also proposed more quantitative electrochemical measurements to characterize the materials corrosion resistance.

Figure 1 summarizes the processing-structure-property relations used in this design of alternative low-cost coinage materials for the US Mint. The processing elements presented in Figure 1 are those defined by the US Mint current manufacturing processes and include casting, rolling, annealing, passivating, upsetting and striking. The property elements in Figure 1 represent the US Mint desired property objectives for the materials. The structure elements are the microstructure features that are needed to achieve the desired property objectives. The lines between the processing, structure, and property elements indicate the relationships between the processing, structure, and property elements for the design. The black lines indicate the processing-structure-property relation highlighted in this design.

The specific processing-structure relations highlighted in this design include the optimization of the composition within the specified casting, rolling, and annealing processes to produce a matrix that does not contain the β phase or allow the precipitation of an ordered phase during cooling. The desired grain size of less than $100\text{ }\mu\text{m}$ is controlled by the annealing time and temperature. It is noted that NIST design process did not include the passivation process, which includes a proprietary method used to add a passivating film to the coins to improve the corrosion and wear resistance. The upsetting and striking processes affect the surface properties of the coin.

The structure-property relations essential for the design also include avoiding the precipitation of the β (bcc phase) and ordered phase to control the electrical conductivity, yield strength,

ductility, and work-hardening rate. The grain size also influences the yield strength and work hardening rate. The amount of Zn in alloy should be optimized to maintain the needed corrosion resistance. Zn may contribute to a dealloying process and degrade the corrosion resistance. The color, cost and density of the coinage materials are all dependent on the alloying concentrations.

Within in this system are several conflicting property objectives that must be optimized within the design process. Lowering the cost of the alloy is a primary design objective; however, this requires reducing the amount of Ni in the alloy, which is a controlling factor in maintaining the desired alloy color. The additions of Mn and Zn to reduce the cost increase the degree of yellow in the alloy color, which is undesirable.

These processing-structure-property relations and optimization of the conflicting property objectives are integrated into a computational design using several CALPHAD-base composition-dependent models, including thermodynamics, electrical conductivity, color, and cost.

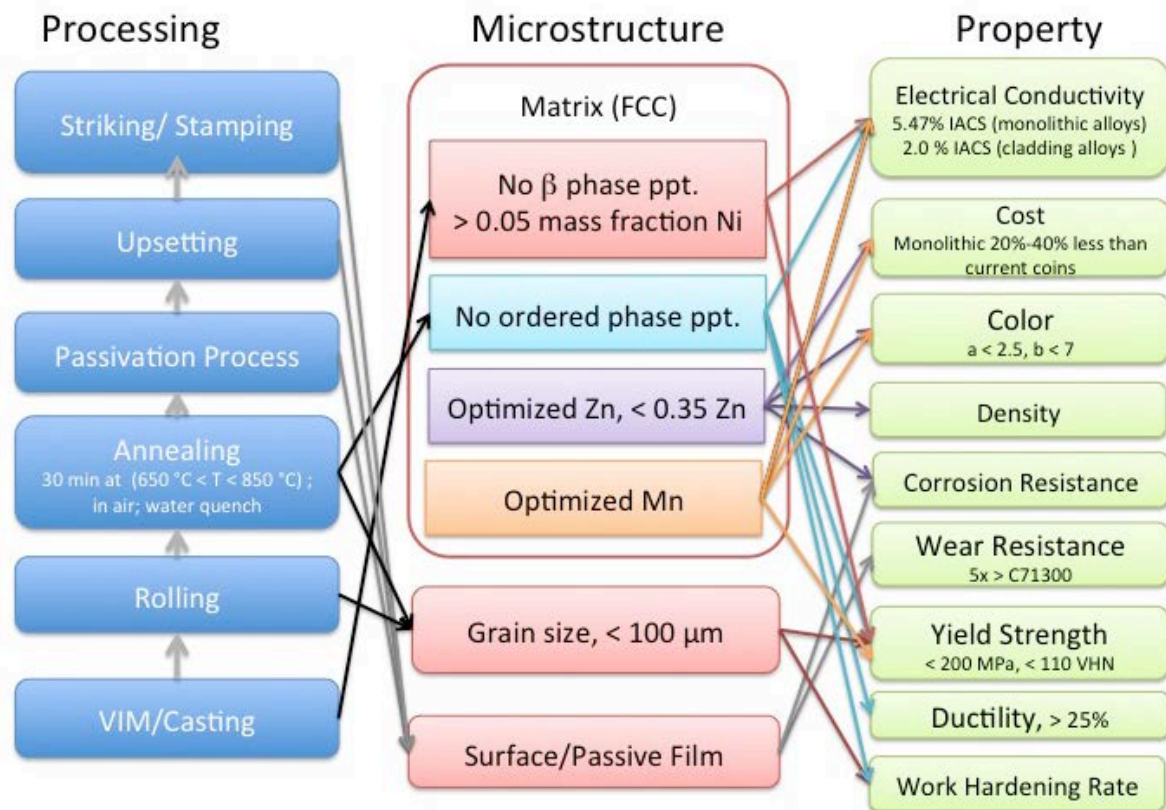


Figure 1. Schematic illustrating the processing-structure-property relations in the design of low cost coinage materials. The arrows represent the relations between the processing and structure and the structure and properties. The arrows in gray are not included in this design process.

2. Experimental Processing & Characterization Methods

During the course of this project, NIST designed and produced all of the needed model and prototype alloys. In addition, much of the characterization of the prototype alloys was completed by NIST. The US Mint was responsible for the wear testing, some corrosion testing and some of the conductivity measurements. NIST produced 1 kg ingots of material in individual lots (or heats) using vacuum induction casting, in the form of rectangular plates with dimensions of about 7.6 cm by 10.2 cm, by 1.3 cm in thickness (for many test alloys, 200 g ingots were produced instead to minimize raw material consumption). The useable portion of the ingot was between 0.5 kg and 0.7 kg. Once melted, the ingots were mechanically processed via rolling to a final thickness of approximately 1.6 mm. A combination of cold rolling (rolling the material while at room temperature), hot rolling (rolling the material while at elevated temperatures), and intermittent heat treatments were used. Annealing in air at temperatures between 650 °C and 850 °C for various times, followed by cooling in a variety of manners, was used as a post processing treatment to simulate the final material condition of potential coins made from the alloys.

NIST employed a variety of characterization methods including optical metallography to study microstructure, x-ray diffraction for phase identification, scanning electron microscopy (SEM) equipped with an energy dispersive x-ray spectrometry (EDS) system for measuring the alloy composition, and Vickers microhardness indentation. The US Mint conducted the initial eddy current electrical conductivity measurements on each lot of material. The conductivity was measured at frequencies of 60 kHz, 120 kHz, 240 kHz, and 480 kHz. To maintain consistency in electrical conductivity measurements, the US Mint measurements were used as the baseline data throughout the course of the project. The US Mint also conducted steam testing and color measurements on selected materials.

Once a final alloy had been designed for each of the three applications, NIST provided the US Mint with approximately 2 kg of material for making and evaluating coins made from the alloys. This characterization included the production of coins, testing the coins in simulated vending machines, and wear-corrosion testing. The US Mint used an experiment designed to simulate ten years or more of service to evaluate the wear-corrosion resistance. The coins were tumbled in a cylindrical drum lined with cloth rotating at 40 revolutions per minute. A simulated sweat solution (described below) was used to keep the cloth damp. The coins were tumbled for several weeks with the mass loss recorded at the end of each week of testing.

NIST evaluated the mechanical properties for the three final alloys using a servohydraulic tensile frame. The critical parameters (i.e., gauge length, gauge width, and thickness) were measured for each tensile specimen with a digital micrometer, prior to testing. A specimen was centered in the hydraulic grips and a 12 mm \pm 0.15 mm extensometer was attached to center of the gauge section. The specimen was then pulled under constant strain rate conditions at a rate of $\dot{\epsilon} = 0.015 \text{ min}^{-1}$ until the limit of the extensometer was reached. The gauge was then removed and the test continued under constant displacement conditions at a rate that achieved a strain rate of $\dot{\epsilon} = 0.25 \text{ min}^{-1}$ until failure.

Electrochemical measurements were conducted by NIST to investigate the corrosion behavior of the final three alloys. Coupons of the each alloy were polished to a 1 μm diamond finish to

remove any mill-scale that may have been present on the surface prior to testing. Exposure tests were conducted in two deaerated solutions under free corrosion potential (FCP) conditions. The first solution, 0.5M sodium sulfate (Na_2SO_4), was used as a reference solution because it is relatively benign with respect to copper alloys. The second solution, simulated human sweat, is a composition used by the US Mint to simulate the in-service behavior of a candidate alloy in service. The simulated sweat had the following composition: 40 g sodium chloride (NaCl), 5 g monobasic sodium phosphate (NaHPO_4), 4 mL lactic acid ($\text{CH}_3\text{CH}(\text{OH})\text{CO}_2\text{H}$), and 4000 mL distilled water (H_2O). A polished coupon was placed in a corrosion cell that was specifically designed to test flat specimens. Nitrogen gas was bubbled through the solution prior to the test. After 15 minutes of bubbling, the flow rate was reduced to a slow stream and continued throughout the exposure test. A computer-controlled potentiostat was configured to measure and record the potential with respect to an Ag/AgCl reference electrode at 1 minute intervals. Each FCP test was conducted for a period of 24 hours.

The FCP is a variable quantity that can be influenced by many factors such as the oxygen concentration in the solution and the active corrosion reactions. While deaerating the solution minimizes the influence of the oxygen on the FCP, it does not eliminate it entirely. For this reason, polarization resistance measurements are a better indicator of the performance for a given alloy in a particular environment. Specimens for these experiments were prepared in the same manner as those used for the FCP measurements. After loading into the corrosion cell, nitrogen gas was slowly bubbled through the solution and the system was allowed to stand for a period of 30 minutes prior to testing. During this time, the FCP was recorded by the potentiostat. Polarization resistance experiments use a potentiostat to fix the specimen potential with respect to a non-polarizable interface, which in this case, was a Ag/AgCl reference electrode. The potential is then scanned through a pre-set range. The potential range for these tests started at the lowest potential [-1.000 V with respect to Ag/AgCl reference electrode (wrt Ag/AgCl)] and then stepped at a 5 mV/s rate to the highest potential (typically 0.125 V wrt Ag/AgCl). The dwell at each potential during the scan was 1 s.

3. Construction of property models for alloy design

An initial set of property models for the thermodynamics, electrical conductivity, color, and processing models were constructed to design the modifications to the C77000 alloy, which is a Cu-Ni-Zn based alloy, and the C997xxx series alloys, which are Cu-Ni-Zn-Mn based.

3.1. Phase diagrams in Cu-Ni-Zn

Figure 2 shows two isothermal sections of the ternary Cu-Ni-Zn phase diagram [2]. At an elevated temperature, 775 °C in Figure 2a, a single phase fcc region exists with a homogeneity range of 0.30 mole fraction Zn over the entire range from Cu to Ni. As temperature decreases, 427 °C in Figure 2b, an ordered L1_2 (Cu_2ZnNi) phase appears (at still lower temperatures another order phase with the L1_0 structure also appears). The composition of C77000 lies directly in the middle of the single-phase L1_2 region of Figure 2b.

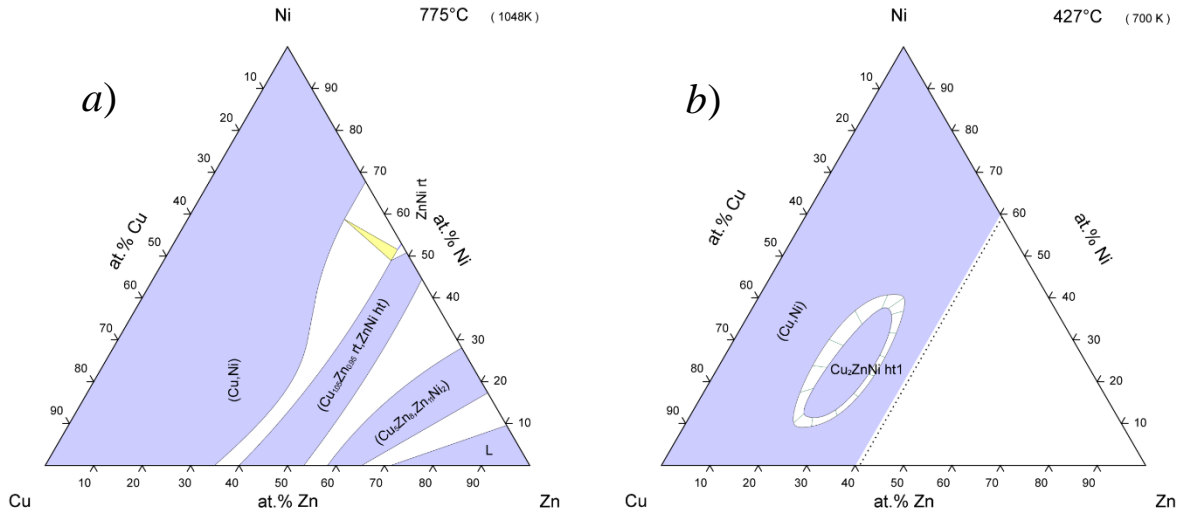


Figure 2: Isothermal sections of the ternary Cu-Ni-Zn phase diagram at a) 775 °C and b) 427 °C [2].

3.2. Phase equilibria modeling in Cu-Ni-Zn-Mn

No ordering reaction occurs in binary Cu-Ni, and the fcc phase is the only phase present at all temperatures. As a result the properties of C71300 and other binary Cu-Ni alloys are fairly insensitive to processing conditions such as annealing temperature/time and cooling rate from the annealing temperature. However, because of the existence of an ordered phase in ternary Cu-Ni-Zn, processing conditions have a significant effect on the final properties of the material. Specifically, the rate at which the material is cooled from temperatures above the ordering reaction must be controlled to produce a material with the desired characteristics. This is because the ordering reaction from fcc to L1₂ occurs very rapidly; and the degree of ordering may vary from completely disordered to fully ordered, depending on the quenching rate from elevated temperatures through the order region of the phase diagram, and finally to near room temperature when the degree of ordering is “frozen” in. As a result, understanding of how processing conditions affect atomic ordering, as evidenced by a change in properties, and controlling those processing conditions so that the final properties of the material are within the specifications, are of paramount importance in designing an alloy based on ternary Cu-Ni-Zn. These relationships are discussed in detail in section 4.1.

In the composition range of interest for designing the two C99-series alloys, the formation of bcc/B2 β -brass becomes a possibility. In the binary Cu-Zn phase diagram, the β -brass phase, with a stoichiometry of roughly Cu_{0.5}Zn_{0.5}, is an ordered B2 phase at low temperatures and disordered bcc above about 450 °C. Whether or not it was ordered in the quaternary Cu-Ni-Zn-Mn alloys was not of concern in the present work, and the phase will simply be referred to as bcc. The bcc phase is considerably harder than the fcc phase, and was also determined during this investigation to be considerably more electrically conductive. It is also yellow in color. As a result, the presence of any bcc is unwanted in the alloys being designed for coinage applications.

Thermodynamic modeling of the quaternary Cu-Ni-Zn-Mn phase diagram was employed to predict expected phases for a given composition. Two thermodynamic descriptions of ternary Cu-Ni-Zn have been published, one by Jiang et al. [3] and one by Miettinen [4]. Miettinen's description is limited to applications with temperatures above 600 °C, and hence does not include the ordered phases that arise at lower temperatures. However, Miettinen has also performed thermodynamic assessments for ternary Cu-Mn-Ni [5] and Cu-Mn-Zn [6] using the same unary and binary subsystems, providing a self-consistent set of the necessary Cu-rich systems for alloy design when Mn is included. For this reason, and because avoidance of bcc was the primary factor in including phase equilibria modeling, Miettinen's thermodynamic descriptions were used in the present alloy design process.

Figure 3 presents two isothermal sections of the quaternary Cu-Ni-Zn-Mn phase diagram at 500 °C and 600 °C for a constant 0.55 mass fraction of Cu. Note that although the Miettinen Cu-Ni-Zn description is valid only for temperatures above 600 °C because atomic ordering is not considered, extrapolation to 500 °C should be sufficiently accurate to determine delineation between the single-phase fcc and two-phase fcc+bcc regions. Both phase diagrams suggest a minimum of 0.03 mass fraction of Ni is needed to produce a completely single-phase fcc microstructure. As a result, a 0.05 mass fraction of Ni was used as a starting point for development of the C99 series of alloys to ensure an alloy would be 100 % single-phase fcc.

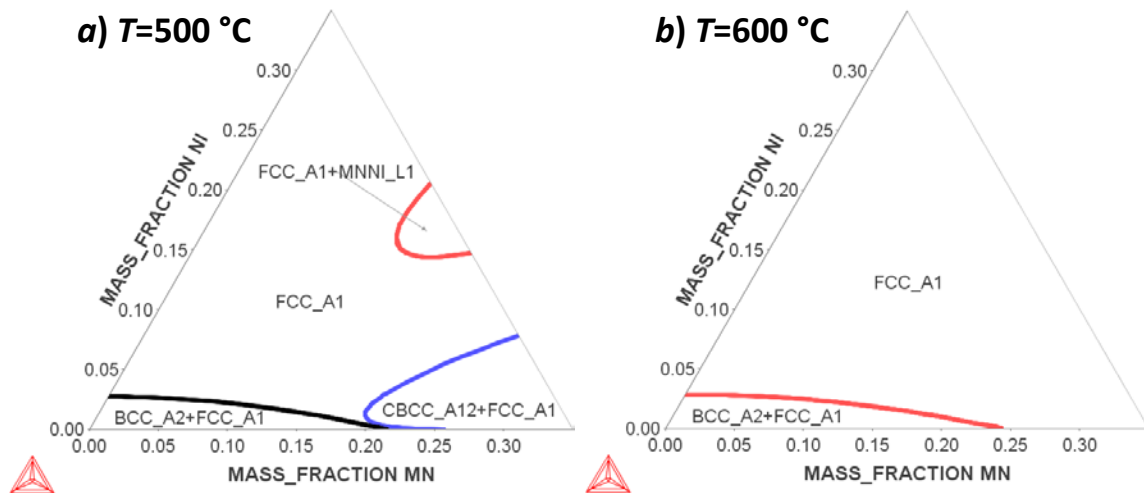


Figure 3: Calculated isothermal sections of the quaternary Cu-Ni-Zn-Mn phase diagram at a) 500 °C and b) 600 °C for a constant mass fraction of 0.55 Cu.

3.3. Conductivity modeling

To ensure that the designed alloys had the desired electrical conductivity matching with C71300, a model was constructed that described the composition dependence of the electrical conductivity in the fcc phase for alloys containing Cu, Ni, Zn, and Mn. The model was constructed using a CALPHAD-type approach [7,8], which starts with the properties of the pure elements, constructs binary models using interaction parameters to describe all available

experimental data; and then combines the binary subsets to construct a ternary description. Any available ternary data can be used to determine ternary mixing terms. Finally a higher component description is built from the ternary subsystems. Mixing interactions beyond ternary are typically negligible and are most often not considered.

In the CALPHAD formulation, a property of a phase ϕ , in this case the electrical resistivity, $\phi\rho$, of a binary A - B system is described by the equation

$$\phi\rho = x_A \phi\rho_A^o + x_B \phi\rho_B^o + x_A x_B \sum_i (x_A - x_B)^i \phi\rho_{AB}^i \quad (1)$$

where x_J is the mole fraction of species J , $\phi\rho_J^o$ is the electrical resistivity of component J in the form of phase ϕ , and $\phi\rho_{AB}^i$ are the i^{th} -order interaction parameters of A and B in the form of phase ϕ that describe the behavior of the electrical resistivity of an A - B solution. Typically the $\phi\rho_J^o$ and $\phi\rho_{AB}^i$ may have a temperature-dependent component, but only room temperature electrical resistivity is considered in the present work. As only the fcc phase is considered in the present electrical resistivity model, ϕ has been omitted from the notation in the remainder of the document. For a ternary system, in addition to the interaction terms for each constitutive binary system, i.e. the summation term of Eq. (1), ternary interaction parameters may also be added if sufficient experimental data exists. These ternary interactions take the form

$$\rho_{ABC} = x_A x_B x_C \sum_{i=0}^2 x_i \rho_{ABC}^i \quad (2)$$

where the x_i in the summation are x_A , x_B , and x_C for i equal to 0, 1, and 2, respectively, and the ρ_{ABC}^i are the ternary interaction parameters for each term in the summation. In some cases a single ternary interaction parameter is specified, in which case all ρ_{ABC}^i are equal and the summation in Eq. (2) collapses to ρ_{ABC}^0 .

Once the composition dependence of the electrical resistivity is optimized via the parameters in Eqs. (1) and (2), the expression is easily converted to conductivity, σ , measured in % IACS. The mole fractions are also converted to mass fractions to facilitate direct comparison of calculated and experimentally measured conductivities on alloys designated via mass fraction of the components.

Experimental data for the electrical conductivity of the fcc phase in binary alloys were taken primarily from ref. [9]. For the Cu-Zn system, the reference reported resistivity data for alloys all across composition space without accounting for what phases were present. In the binary phase diagram, β -brass and other phases are present above about 0.40 Zn mass fraction; so only resistivity data for composition between 0 and 0.40 mass fraction Zn were included.

Additionally, only room temperature experimental data measured on fully annealed and quenched materials were used wherever possible. For instance, Mn-Ni alloys have a tendency to form order phases at lower temperatures. Binary alloys near a 0.25 mole fraction of Mn exhibit a lower resistivity after being annealed at low temperature (allowing an ordered structure to form) when compared to the same composition annealed at high temperature and rapidly quenched to room temperature to avoid ordering. Thus, the quenched sample data was used to maintain a consistent crystal structure for all systems.

No experimental data was available for two binary systems, Ni-Zn and Mn-Zn. The Ni-Zn phase diagram is similar to that of Cu-Zn, and Cu and Ni are chemically similar; so the electrical conductivity in binary Ni-Zn was assumed to behave similar to that of Cu-Zn, and was modeled as such. For the Mn-Zn system, the electrical resistivity was assumed to behave similarly to the three other Mn-binary systems and a parabolic shape with a maximum in resistivity near an equi-atomic (50/50) composition was assumed. A single mixing parameter is used for each of these systems; and the values of this parameter were very similar for all systems. Therefore, for Mn-Zn a single mixing parameter was used and was given a value similar to those for the other Mn-containing binary systems. Table 1 presents the optimized parameters for all the systems studied during the course of this project. Note that since the value the electrical resistivity of fcc Zn could not be determined, the value of hcp Zn was used instead.

Table 1: Optimized parameters used to describe the composition dependence of the electrical resistivity of the fcc phase in the quaternary Cu-Ni-Zn-Mn system. The electrical resistivity of HCP Zn was used because no value for fcc Zn could be found.

System	ρ_f^o ($\mu\Omega\cdot\text{cm}$)	$\rho_{AB(C)}^0$	$\rho_{AB(C)}^1$	$\rho_{AB(C)}^2$
Cu	1.72			
Mn (fcc)	23			
Ni	6.58			
Zn (hcp)	5.45			
Cu-Mn		653.23	-394.72	
Cu-Ni		179.12	-10.61	-59.33
Cu-Zn		4.49	17.85	12.93
Mn-Ni		419.94	192.11	
Mn-Zn		300		
Ni-Zn		10	10	
Cu-Mn-Ni		-258.34		
Cu-Mn-Zn		26.95		
Cu-Ni-Zn		-108.43	937.97	435.36

Figure 4 presents the calculated composition dependent electrical conductivity (in % IACS) for each of the six binary subsystems of the quaternary Cu-Ni-Zn-Mn system of interest. There is good agreement between model and experiment for the four systems where experimental data are available. As mentioned above, the model for Ni-Zn is reasonable considering the chemical similarity between Ni and Cu; while the Mn-Zn description is consistent with the other two Mn-containing systems.

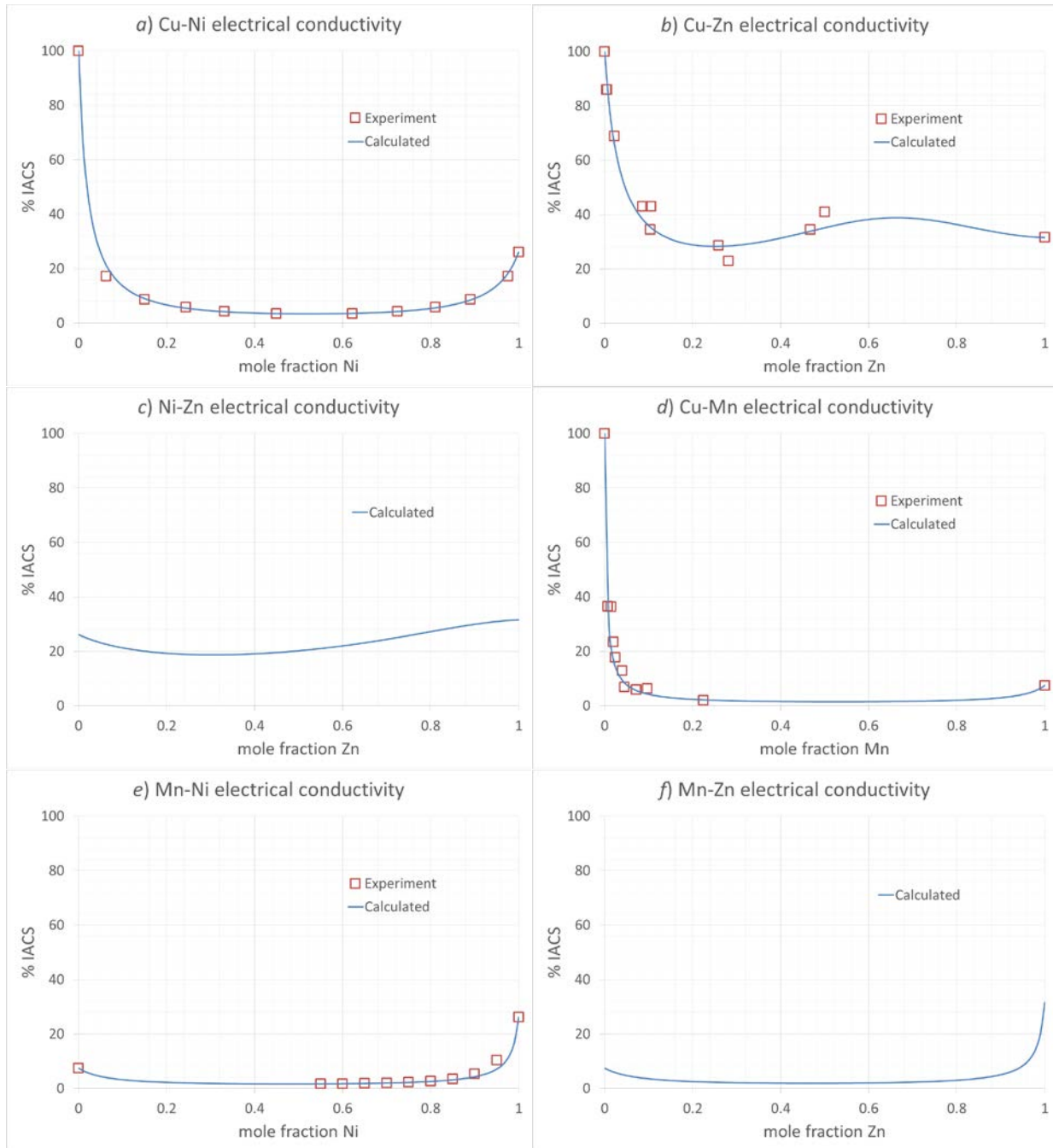


Figure 4: Composition dependent electrical conductivity behavior calculated using the model built in the present work compared to the experimental data for the six binary subsystems of the Cu-Ni-Zn-Mn system.

Ternary experimental data were quite sparse. Initially, only the pure ternary Cu-Ni-Zn system was considered. The only available experimental data in this system were for commercial ternary Cu-Ni-Zn alloys on various materials suppliers' websites [10-13]. These alloys are not true ternaries as they contain industrially added impurity elements (less than 0.01 mass fraction) and other minor alloying elements (less than 0.03 mass fraction). Many of these commercial alloys contain elements such as Pb, Fe, Al, or Sn in quantities on the order of 0.001 mass fraction. The electrical conductivity data of commercial alloys were only used in the ternary

assessment of the model if they contain no additional element in quantities greater than 1 % mass fraction (i.e. no minor alloying elements). It is also noted that the material processing history of the alloys from which conductivity values were available was unknown, further increasing the uncertainty of these data. Therefore, once the first few NIST model alloys were produced and characterized, the measured conductivity values from these alloys were included in the ternary data set to improve the accuracy of the ternary description. Table 2 lists the commercial alloys in the Cu-Ni-Zn-Mn family that have reported conductivities. Note that many contain elements such as Pb, Fe, Al, or Sn in quantities on the order of 0.01 mass fraction.

Table 2: List of commercial alloys within the Cu-Ni-Zn-Mn family (some with additional alloying elements) for which conductivity data has been reported [7-10].

Alloy	Type	Composition (mass fraction time 100)							Conductivity, % IACS [ref.]			
		Cu	Ni	Zn	Mn	Other	[7]	[8]	[9]	[10]		
C66700	Wrought	68.5-71.5	0	Bal (30)	0.8-1.5	<0.07Pb, <0.1Fe	17					
C66900	Wrought	62.5-64.5	0	Bal (24.5)	11.5-12.5	<0.05Pb, <0.25Fe	3.4					
C66925	Wrought	Bal	0.01-3.5	17-21	8-11	<0.05Pb, <0.5Fe, <0.5Sn, <0.25Al, <0.01Co	4.5					
C66930	Wrought	Bal (80.25)	0	0	19-20.5	<0.02Ni, <0.05Zn, <0.02Pb, <0.05Fe, <0.05Sn, <0.02P	2					
C66950	Wrought	Bal (69.75)	0	14-15	14-15	<0.01Pb, <0.5Fe, 1-1.5 Al	3.4					
C69250	Wrought	Bal (82.5)	2-3	7.5-8.5	5-6	<0.5Pb, <0.2Fe, <0.2Sn, 1-2Al, <0.1Si	6					
C70600	Wrought	Bal (88.6)	9-11	<1	<1	<0.05Pb, 1-1.8Fe	9.1					
C71000	Wrought	Bal (79)	19-23	<1	<1	<0.05Pb, <1Fe	6.5					
C71500	Wrought	Bal. (68.3)	29-33	<1	<1	<0.05Pb, 0.4-1Fe	4.6					
C73100	Wrought	Bal (76)	4-6	18-20	<0.5	<0.05Pb, <0.1Fe, <1Sn	7.5					
C73500	Wrought	70.5-73.5	16.5-19.5	Bal (10)	<0.5	<0.09Pb, <0.25Fe	6.5					
C74500	Wrought	63.5-66.5	9-11	Bal (25)	<0.5	<0.09Pb, <0.25Fe	9	9				
C75200	Wrought	63-66.5	16.5-19.5	Bal (18)	<0.5	<0.05Pb, <0.25Fe	6	6	6	6		
C75400	Wrought	63.5-66.5	14-16	Bal (20)	<0.5	<0.10Pb, <0.25Fe	7	6	7			
C75700	Wrought	63.5-66.5	11-13	Bal (23)	<0.5	<0.05Pb, <0.25Fe	8		8			
C76200	Wrought	57-61	11-13.5	Bal (29)	<0.5	<0.09Pb, <0.25Fe	9		9			
C76390	Wrought	59-63	23-26	Bal (13.05)	<0.5	0.8-1.1Pb, <0.25Fe, 0.4-0.6Sn	4					
C76400	Wrought	58.5-61.5	16.5-19.5	Bal (20)	<0.5	<0.05Pb, <0.25Fe		5.7				
C76800	Wrought	47.5-50	8-9.5	Bal (37)	4.5-6.5	<0.09Pb	4.4					
C77000	Wrought	53.5-56.5	16.5-19.5	Bal (27)	<0.5	<0.05Pb, <0.25Fe	5.5	5.7	5.5	5.5		
C77100	Wrought	52-56	9-12	Bal (35.5)	<9	<0.03Pb	7.6					
C78270	Wrought	65-68	4.5-6	Bal (23)	<0.5	1-1.8Pb, <0.35Fe	10					
C79350	Wrought	59-63	23-26	Bal (13.05)	<0.5	0.8-1.1Pb, <0.25Fe, 0.4-0.6Sn	4					
C79860	Wrought	42.3-43.7	11.8-12.7	Bal (37.2)	5.6-6.4	1.3-1.8Pb, <0.2Fe, <0.1Sn, <0.005P, <0.06Si	5					
C86800	Cast	53.5-57	2.5-4	Bal (36.5)	2.5-4	<2Pb, 1-2.5Fe, <1Sn, <2Al	9					
C99700	Cast	>54	4-6	19-25	11-15	<2Pb, <1Fe, <1Sn, 0.5-3Al	3					
C99710	Cast	>60	4-6	19-25	11-15	<0.09Pb, <1Fe, <1Sn, <1Al	10					
C99750	Cast	55-61	<5	17-23	17-23	0.5-2.5Pb, <1Fe, 0.25-3Al	2					

Figure 5 presents a 3D representation of the final electrical conductivity model constructed for ternary Cu-Ni-Zn system. As a point of reference the calculated conductivity of the ternary analog of C77000 (Cu-18Ni-27Zn) is 5.73 % IACS using the model, while the values reported by material suppliers ranged from 5.5 % IACS to 5.7 % IACS. When Mn is included in the model (described below), an alloy also containing 0.003 mass fraction of Mn (the typical content in the commercial alloy) is calculated to have a conductivity of 5.53 % IACS. For comparison with experiment, the measured conductivity of the pure ternary analog produced at NIST was 5.8 % IACS, while that of one also containing 0.003 mass fraction Mn was 5.7 % IACS.

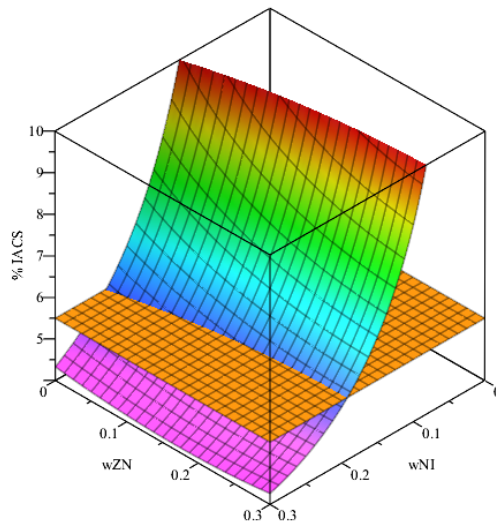


Figure 5: Composition dependent model of electrical conductivity constructed for the ternary Cu-Ni-Zn system shown as function of the mass fraction of Zn and Ni (multicolored inclined space curve. The orange plane is a constant conductivity of 5.5 % IACS.

Mn is a primary alloying element in the two C99 series alloys. Initial conductivity testing at NIST confirmed the important effect that Mn has on the alloy conductivity. This was observed even in the commercial ternary C77000-derivative, where the composition of Mn is less than 0.01 mass fraction. Thus, Mn was included the electrical conductivity model for all of the design alloys. The only available data for ternary Mn-containing alloys were for a handful of commercial ternary Cu-Zn-Mn alloys (C6xxxx alloys in Table 2). No data were available for the Cu-Ni-Mn system. Conductivity data for the quaternary system Cu-Ni-Zn-Mn were available base on four commercial alloys quaternary alloys, containing all four elements in concentrations greater than 0.01 mass fraction and less than 0.001 mass fraction for all other alloying additions. With limited data available to calibrate the model with Mn included, a series of quaternary alloys with the composition $\text{CuNi}_5\text{Zn}_{40-x}\text{Mn}_x$ (where x is 5, 10, 15, 20, and 25) were produced to provide additional experimental data (the measurements of these alloys will be summarize in subsequent sections with the rest of the experimental results). The electrical conductivity model was calibrated by first optimizing the ternary Cu-Zn-Mn description, for which limited data were available, and then by using the commercial and experimental quaternary data to determine the mixing parameters for the Cu-Ni-Mn system. No quaternary fitting was performed. The resulting description of electrical conductivity in the quaternary system was used to determine

composition tolerances for the C77000-derivative, and for the design of the two C99 series alloys. The model was refined slightly as additional experimental data were collected; however, the final values of the parameters changed very little from the initially optimized system. The optimized results of the assessment process (expressed as electrical resistivity) are presented in Table 1.

3.4. Color modeling

Color properties of the alloy are important for this application, as the new alloys should retain same color properties as the currently used materials. Lahiri et al.[14] presented a preliminary model of the composition dependence of color in the Cu-Mn-Zn as in Figure 6, a diagram of expected color (white, yellow, or red) for alloys in the Cu-Mn-Zn ternary system. Figure 6 provides a reasonable starting point for predicting what to expect of a given ternary Cu-Mn-Zn composition. The diagram can even be extended to include Ni if the Ni is assume to behave like Mn in determining color and the Mn and Ni concentrations are summed together to give a “quasi” Mn-content. However, in considering coin alloy color, a more quantitative description of color was needed.

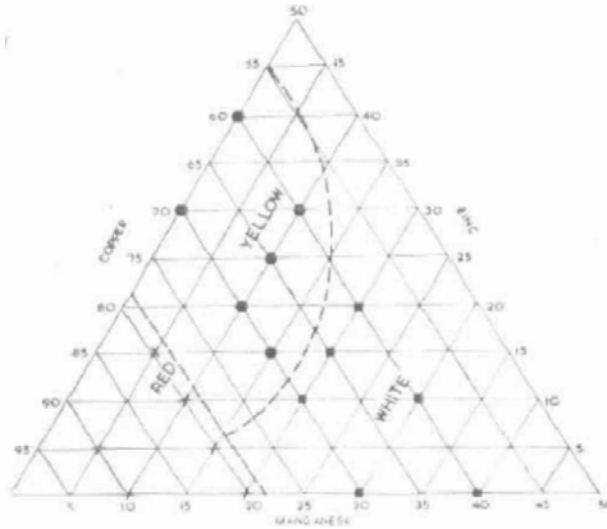


Figure 6: Map of expected color for alloys in the Cu-Mn-Zn ternary system [14]

For the purpose of coinage alloys, the US Mint has developed quantitative standards, based on the Commission of Illumination (CIE) $L^*a^*b^*$ color space, with dimension L^* for lightness, and a^* and b^* for the color-opponent dimensions. In the context of Cu-based coin alloy color, a^* is essentially a measure of “redness” while b^* is a measure of “yellowness”. A particular hue can be represented as a vector, i.e. $[L^*, a^*, b^*]$ (Lab for short). Although Lab is meant as quantitative measurement of color, the values of each dimension are quite dependent on material history and measurement conditions. For instance, separate tests on C71300 performed during the course of this project produced significantly difference results. Samples that had been freshly ground with 600 grit SiC grinding paper exhibited a Lab of [78, 1.1, 5.4]; while the measured Lab of cold-rolled C71300 was [73, 1.9, 8.7]. Measurements performed on US 5-cent coins gave yet another result of [79, 1.0, 5.1]. The wide variation in measured colors is due primarily to reaction of the

material surface with the environment (i.e. oxidation), although surface preparation may play a role as well. There are no published *Lab* values for alloys, so data collected during the course of the project were used to construct and refine an empirical model describing color as a function of composition.

The first iteration of the description was adopted from ref. [15] and modified by replacing the Mn concentration variable with the sum of the Ni and Mn concentrations. The equation used is given by

$$b^* = A + Bw_{Zn} + Cw_{Zn}^2 + D(w_{Mn} + w_{Ni}) + E(w_{Mn} + w_{Ni})^2 + Fw_{Zn}(w_{Mn} + w_{Ni}) \quad (3)$$

where the w_j is the mass fraction of component J , and A through F are fitting parameters, and are given in Table 3. Figure 7 clearly shows that although Eq. (3) captures the general trend in the color, i.e. as the ratio of Mn plus Ni concentration to Zn concentration increases b^* decreases. However the calculated values are consistently lower than the measured values, so a more accurate description of color was needed.

Table 3: Assessed parameters for the two color models considered for alloy design, described by Eqs. (3) and (4).

Model	A	B	C	D	E	F	G	H
Eq. (3)	14.624	246	-38.5	-829	135.2	-56.5	-	-
Eq. (4)	0	-41.38	146.5	23.47	-319.8	77.85	-117.2	-1868

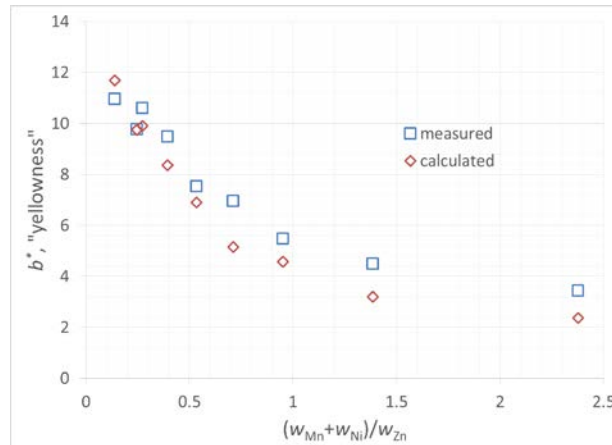


Figure 7: The first iteration of the empirical color model use in the design of the C99 monolithic alloy compare with experimentally measured values of b^* .

The second-generation color model was based on a CALPHAD-type polynomial function of the composition variables, given by the equation

$$b^* = A + Bw_{Mn} + Cw_{Mn}^2 + Dw_{Ni} + Ew_{Ni}^2 + Fw_{Zn} + Gw_{Zn}^2 + Hw_{Mn}w_{Ni}w_{Zn} \quad (4)$$

The optimization of Eq. (4) to the limited amount of data during the early stages of investigation resulted in unrealistic values for the Mn and Ni terms (i.e. increasing Mn or Ni concentration

increased b^* , which is certainly not the case). The term A was therefore initially set to zero, which alleviated the issue. As subsequent data was collected, the color model could be further refined. Again however, because of the volatility of color measurement the improvement in accuracy was minimal. Therefore the initial optimization of Eq. (4) was used for the majority of the alloy design process. The fitting parameters for this initial optimization of Eq. (4) are given in Table 3.

3.5. Cost modeling

As the material cost was the primary design objective, it was also included as a design parameter. Only the cost of raw materials was considered, i.e. no change the cost producing the material ultimately used by the US Mint costs was considered. The price per kg of the pure elements when the project began were used to compute alloy cost, given by the equation

$$\text{cost (\$/kg)} = 7.8w_{\text{Cu}} + 2.3w_{\text{Mn}} + 14.5w_{\text{Ni}} + 2.1w_{\text{Zn}} \quad (5)$$

The cost of C71300 using Eq. (5) is \$9.46 per kg. The Ni largest influence on the overall cost and Cu has the second largest impact on the alloy cost. The primary design objective was to replace as much Ni as possible with Zn and Mn, while maintaining the desired material properties, the conductivity in particular.

4. Alloy design of modified C77000 alloy

4.1. Processing-structure-property relationships: Annealing Effects

As indicated in the design schema in Figure 1, the atomic ordering that occurs in Cu-Ni-Zn alloys is controlled by the processing conditions, and has a pronounced effect on the properties of the material, specifically the electrical conductivity and hardness. Experiments were conducted to determine the effect of annealing temperature, time, and cooling rate on the electrical conductivity and the hardness. First, cooling rate effects were investigated by exposing samples of commercial C77000 in the as-received condition to a heat treatment of 30 min at 750 °C followed by cooling at three different rates: 1) water quenching, 2) air cooling where the sample was removed from the furnace set aside to allow cooling to room temperature, and 3) furnace cooling where the furnace was turned off at the end of the 30 min anneal which allowed the specimen to slowly cool to room temperature overnight.

Additionally, samples of as-cold-rolled C77M-1 and a NIST-produced analog of C77000 were subjected to heat treatments for 30 min at temperatures between 675 °C and 850 °C, as well as for times between 10 min and 60 min at a temperature of 750 °C, followed by a water quench. These tests were designed to study the effects of annealing temperature and time of electrical conductivity and Vickers microhardness.

Figure 8 presents the results of the annealing temperature studies. Figure 8a demonstrates that a faster cooling rate results in a higher electrical conductivity and a lower hardness. This is due to

the increased atomic ordering that occurs during the slow cooling process. Fortunately, current US Mint production protocols use a water quenching process; therefore, a new alloy can be designed around this quenching rate.

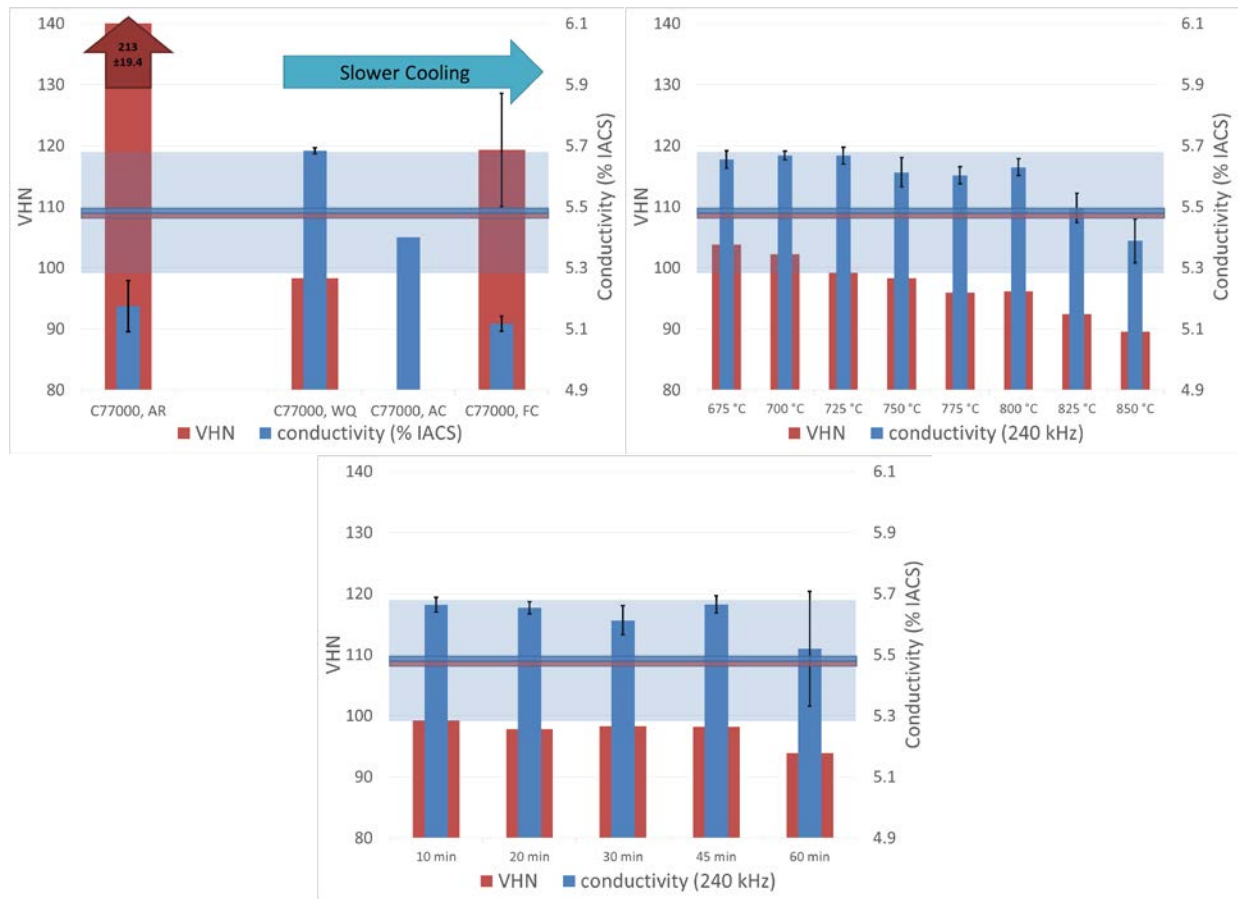


Figure 8: Effects of processing conditions on the electrical conductivity of C77000 and C77M-1: a) cooling rate effect, b) annealing temperature effect, c) annealing time effect. The blue bar and blue shaded area represent the target electrical conductivity range; while the red bar is the maximum allowable hardness design specification. Error bars represent the standard deviation of at least five measurements.

Figure 8b indicates that for an annealing time of 30 min, the microhardness steadily decreases as the temperature is increased. This is an expected result due to the increased degree of recovery, recrystallization and grain growth at the higher temperatures. In contrast, the increased annealing temperature has little effect on the conductivity between 675 °C and 800 °C; however, the conductivity exhibits a significant decrease above 800 °C. While the reason for this decrease in conductivity is not entirely clear, there are two possible explanations for this behavior: The first is rapid grain growth at temperatures above 800 °C, and the second is residual plastic deformation in the microstructure that may not be fully removed until the temperature is above 800 °C.

Figure 9 illustrates the effect of annealing temperature on the microstructure of C77M-1. As expected, the grain size increases with increasing annealing temperature. Also striations are

visible in the micrographs at the annealing temperatures of 700 °C, 750 °C, and 800 °C. These striations occur along the rolling direction and become more prevalent as the annealing temperature decreases. The striations are not observed after annealing at 850 °C. The source of these striations is not clear; however, it is likely that they are produced by residual plastic deformation and are only present near the surface. Despite the presence of these striations, C77M-1 can be processed at temperatures between about 725 °C and 800 °C and the resulting material will have reasonably constant conductivity and microhardness values. This indicates that this alloy exhibits suitable mechanical properties for the US Mint coin production requirements.

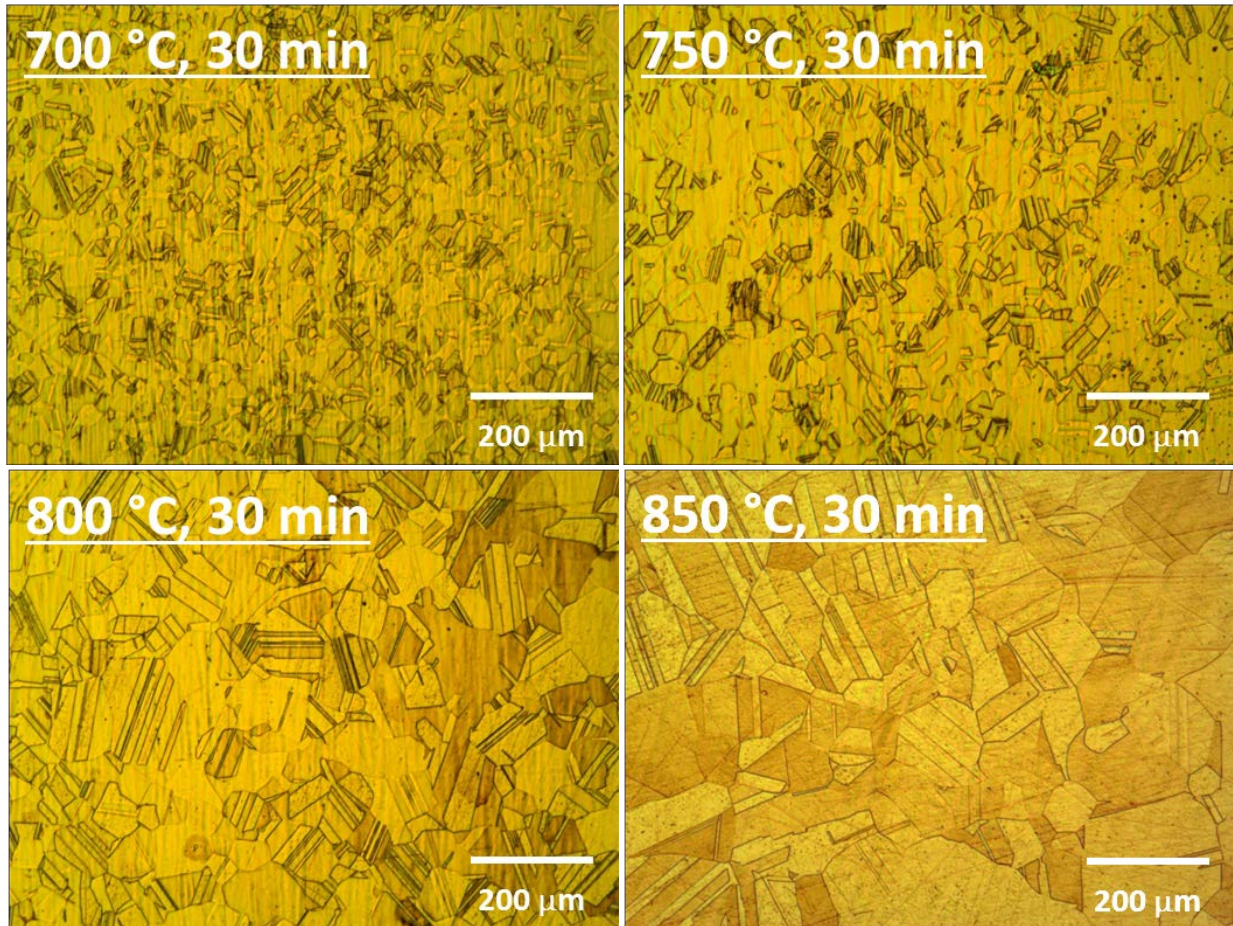


Figure 9: Effect of annealing temperature on the microstructure of C77M-1 for a fixed annealing time of 30 min.

Figure 8c shows that for times between 10 min and 45 min at 750 °C, the annealing time has little effect on the conductivity or on the microhardness. This suggests that the majority of the annealing effect occurs very early on in the heat treatment process. After annealing for 60 min both the conductivity and microhardness begin to decrease. This is likely a result of the same mechanism discussed above for elevated annealing temperatures. Figure 10 presents the resulting microstructures for annealing times between 10 min and 60 min at 750 °C. In this figure, the grain size increases with increasing annealing time. Also, the prominence of the striations in the microstructure generally decreases with increasing annealing time. While

striations are still visible in the 750 °C, 60 min annealed sample (despite the observed decreases in conductivity and microhardness), it is possible that these annealing conditions lie at the onset of the same mechanism that produces the decrease in hardness and conductivity. The hardness and conductivity values of the sample annealed for 60 min at 750 °C are similar to those annealed for 30 min at 825 °C, where the decreases are first observed (Figure 8b).

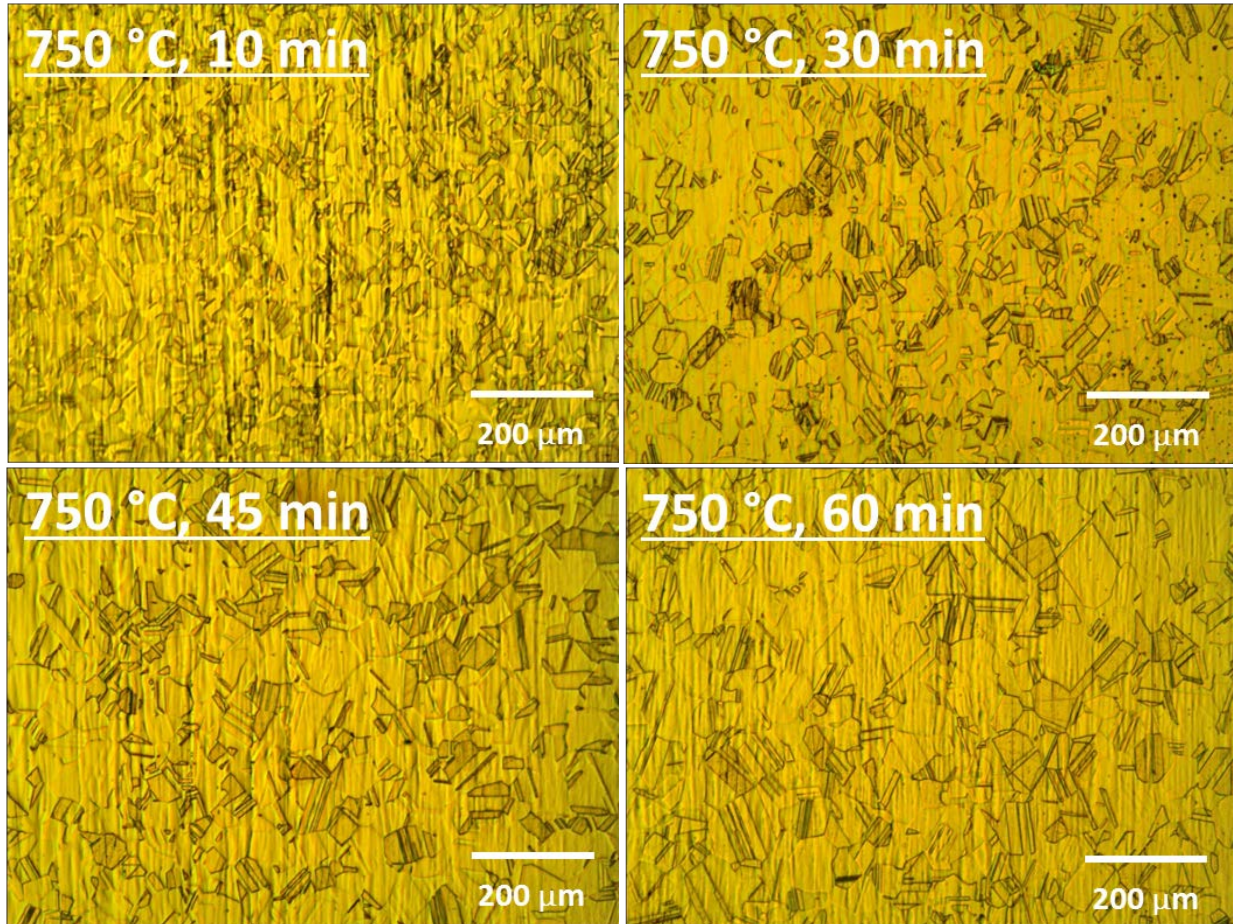


Figure 10: Effect of annealing time on the microstructure of C77M-1 for a fixed annealing temperature of 750 °C.

The results of the above annealing analysis are essential to establish boundaries on potential manufacturing processing conditions. They also demonstrate that certain processing parameters, namely temperature and annealing time, could be varied slightly during the course of production. US Mint production facilities have a fixed annealing time of 30 min and water quenching, but temperature can be varied from roughly 650 °C to 850 °C. Based on this processing window for the annealing, a standard post-production (after casting and rolling to the specified thickness) heat treatment regimen of 30 min at 750 °C, followed by water quenching was chosen as the design condition for the potential prototypes. However, during the process of rolling the as cast ingot into sheet, the time and temperature of intermediate annealing steps were optimized to produce a final sheet material of the highest quality possible. The above results were used to both guide the processing optimization, and to ensure that the final product (i.e., annealed for the

standard 30 min at 750 °C, followed by a water quench) would exhibit the same materials properties, regardless of the intermediate steps between cast ingot and rolled sheet.

4.2. Reproduction of C77000

The first identified task in developing a modified C77000 alloy was to reproduce the commercial alloy using the NIST processing methods. NIST produced 2 kg of material for US Mint to test. C77000 is a commercial ternary with the nominal composition Cu-0.18Ni-0.27Zn (by mass fraction). All minor and tramp alloying elements (particularly Mn and Fe) were initially neglected and the first NIST-produced alloy was a pure ternary analog designated C77T². The composition and properties of C77T-5, -6, -7, -9, and -11 are presented in Table 4 for a variety of processing history conditions, along with the properties of all alloys studied during the development of the modified C77000 alloy. The C77T-6, -7, -9, and -11 were produced for testing by the US Mint, but were never used.

The electrical conductivity of the C77T alloys in the annealed and water quenched state (A-WQ) are consistently between 5.8 % IACS and 6.2 % IACS, which is higher than that of C77000 (5.683 % ± 0.003 % IACS). The reason for this difference was identified when Mn is added to the composition. The C77M-1 included 0.003 mass fraction Mn and had a lower A-WQ conductivity (5.673 % ± 0.019 % IACS), which was very similar to that of C77000. Additionally, comparison the electrical conductivity of C77M-1 and C77000 were similar when the processing conditions were varied. C77M-1 was considered a successful reproduction of the commercial alloy and identified the significant impact of Mn on the electrical conductivity. All future design work included the effect of Mn on the conductivity.

² The letter “T” was used to designate test or ternary. For the first few alloys, designation letters were assigned based on a characteristic of the alloy. For instance, C77M contained Mn. Starting with C77D, and continuing into the C99 series development, letter designations were assigned to alloys in alphabetical order as new compositions were produced. The number following a given alloy designation signifies the heat (melt) number.

Table 4: Summary of alloys produced during the development of the modified C77000 alloy C77D. All compositions are given in mass fraction multiplied by 100. Notes: a) required Zn mass multiplied by 1.05 to account for evaporation; b) annealing performed at 700C for 40 min; c) annealing performed at 725 °C for 1hr; d) composition measured externally by Laboratory Testing Inc.; e) used for mechanical tests only; f) performed at the US Mint, no standard deviation provided; g) measured at 480 kHz. Condition legend: in use-current US 5-cent coins; A-annealed; WQ-water quenched; FC-furnace cooled; AR-as received; AirC-air cooled; AC-as cast; CRA-cold rolled with intermediate annealing steps; OQ-oil quenched; WR-warm (hot) rolled; CR-cold rolled.

Date	Designation (condition)	Nominal Composition (mass fraction time 100)	Mass (g)	Comments	Measured Composition (mass fraction time 100)				Conductivity 240Hz (IACS)	Hardness VHN100 (kg/mm ²)
					Ni	Zn	Mn	Fe		
N/A	C71300 (in use)	Cu-25Ni-0.3Mn			25.77±0.27		0.33±0.05		5.472±0.100	101.6±11.1
	C71300 (A-WQ)							5.555±0.008		
	C71300 (A-FC)							5.581±0.008		
N/A	C77000 (AR)	Cu-18Ni-27Zn-0.3Mn	NA		18.40±0.18	25.82±0.28	0.29±0.05		5.175±0.021	213.3±9.7
	C77000 (A-WQ)	Cu-18Ni-27Zn-0.3Mn	NA					5.683±0.003		
	C77000 (A-AirC)	Cu-18Ni-27Zn-0.3Mn	NA					5.400 ^f		
	C77000 (A-FC)	Cu-18Ni-27Zn-0.3Mn	NA					5.117±0.006		
4/2/2014	C77T-5 (AC)	Cu-18Ni-27Zn	750	a,b					5.383±0.047	
	C77T-5 (CRA-A-OQ)				18.75±0.43	25.80±0.32			5.859±0.022	105.0±3.6
	C77T-5 (CRA-A-FC)								5.431±0.023	114.5±3.2
4/23/2014	C77M-1 (AC)	Cu-18Ni-27Zn-0.3Mn	750	a,b					5.143±0.049	
	C77M-1 (CRA-A-OQ)				18.13±0.24	26.43±0.17	0.29±0.02		5.673±0.019	113.7±2.7
	C77M-1 (CRA-A-FC)								5.238±0.042	118.0±5.8
5/9/2014	C77T-6 (AC)	Cu-18Ni-27Zn	1000	a,c					5.481±0.050	
	C77T-6 (WR)				17.04±0.17	27.99±0.15			5.883±0.015	166.9±4.4
	C77T-6 (WR-A-WQ)								5.869±0.006	105.2±2.0
5/12/2014	C77T-6 (WR-A-FC)								5.249±0.005	119.3±4.6
	C77T-7 (AC)	Cu-18Ni-27Zn	1000	a,c					5.578±0.142	
	C77T-7 (WR)				16.65±0.45	28.54±0.24			6.085±0.021	187.6±5.2
5/19/2014	C77T-7 (WR-A-WQ)								5.945±0.003	105.4±2.0
	C77T-7 (WR-A-FC)								5.440±0.007	112.4±7.2
	C77T-9 (WR)	Cu-18Ni-27Zn	1250	a,c	16.97±0.48	27.84±0.16			6.175±0.047	182.5±6.9
5/21/2014	C77T-9 (WR-A-WQ)								6.042±0.016	99.0±2.8
	C77T-11 (WR)	Cu-18Ni-27Zn	1250	a,c	16.95±0.21	28.20±0.17			5.980±0.018	193.7±3.1
	C77T-11 (WR-A-WQ)								5.868±0.010	105.1±3.0

Table 4 (cont.): Summary of alloys produced during the development of the modified C77000 alloy C77D. All compositions are given in mass fraction multiplied by 100. Notes: a) required Zn mass multiplied by 1.05 to account for evaporation; b) annealing performed at 700C for 40 min; c) annealing performed at 725 °C for 1hr; d) composition measured externally by Laboratory Testing Inc.; e) used for mechanical tests only; f) performed at the US Mint, no standard deviation provided; g) measured at 480 kHz. Condition legend: in use-current US 5-cent coins; A-annealed; WQ-water quenched; FC-furnace cooled; AR-as received; AirC-air cooled; AC-as cast; CRA-cold rolled with intermediate annealing steps; OQ-oil quenched; WR-warm (hot) rolled; CR-cold rolled.

Date	Designation (condition)	Nominal Composition (mass fraction time 100)	Mass (g)	Comments	Measured Composition (mass fraction time 100)				Conductivity		Hardness VHN100 (kg/mm ²)
					Ni	Zn	Mn	Fe	240Hz (IACS)	480kHz (IACS)	
7/7/2014	C77D-2 (AC)	Cu-19Ni-26Zn-0.3Mn	1250		19.51±0.16	26.09±0.23	0.27±0.04		5.787±0.024	248.5±6.9	
	C77D-2 (CR)							5.524±0.056	104.6±3.7		
	C77D-2 (CR-A-WQ)										
7/10/2014	C77D-3 (AC)	Cu-19Ni-26Zn-0.3Mn	1000	d	18.97±0.57	26.41±0.38	0.25±0.03		5.726±0.043	247.0±5.8	
	C77D-3 (CR)				18.86	25.33	0.27			103.1±3.1	
	C77D-3 (CR-A-WQ)										
7/11/2014	C77D-4 (AC)	Cu-19Ni-26Zn-0.3Mn	1000		18.89±0.50	26.30±0.21	0.28±0.04				
	C77D-4 (CR)				18.50	25.47	0.27		5.747±0.034	248.8±8.1	
	C77D-4 (CR-A-WQ)									100.6±2.8	
7/10/2014	C77D-5 (AC)	Cu-19Ni-26Zn-0.3Mn	1000		19.39±0.33	26.08±0.31	0.24±0.04				
	C77D-5 (CR)				18.98	25.55	0.28		5.687±0.010	250.2±6.4	
	C77D-5 (CR-A-WQ)									103.0±2.8	
7/13/2014	C77D-6 (AC)	Cu-19Ni-26Zn-0.3Mn	1000		19.51±0.32	26.05±0.32	0.27±0.03		5.720±0.073	246.8±2.9	
	C77D-6 (CR)									105.7±2.8	
	C77D-6 (CR-A-WQ)										
8/4/2014	C77D-7 (AC)	Cu-19Ni-26Zn-0.3Mn	1000	e							
	C77D-7 (WR)										
	C77D-7 (WR-A-WQ)										
9/3/2014	C77E-1 (AC)	Cu-19Ni-26Zn-0.3Mn-0.25Fe			18.98±0.38	25.50±0.20	0.28±0.02	0.20±0.05			
	C77E-1 (WR)				19.04	24.28	0.30	0.17	5.570±0.030		
	C77E-1 (WR-A-WQ)								5.409±0.031		
9/22/2014	C77G-1 (AC)	Cu-20Ni-24Zn-0.5Mn-0.2Fe			20.07±0.18	23.64±0.23	0.45±0.03	0.16±0.04			
	C77G-1 (WR)				20.63	20.05	0.48	0.17	5.221±0.037 ^f		
	C77G-1 (WR-A-WQ)										
9/25/2014	C77H-2 (AC)	Cu-18Ni-28Zn-0.2Mn			18.19±0.34	27.59±0.24	0.20±0.04				
	C77H-2 (WR)				17.97	26.43	0.19		5.754±0.039 ^g		
	C77H-2 (WR-A-WQ)										

4.3. Design and characterization of C77D, the modified C77000

4.3.1. Alloy development

The design of a modified C77000 alloy was initiated once C77000 was successfully reproduced on the laboratory level, and all the necessary modeling and experimental tools were validated. The goal of creating the modified C77000 was to optimize the alloy conductivity to match that needed for the US Mint application. The color of C77000 is actually less yellow than C71300 so it was not considered in this design. The cost also was not a design consideration during this phase of the project because the raw materials cost of C77000 is already approximately 20 % less than C71300. Thus, conductivity was the primary focus of the alloy design, with mechanical, corrosion, wear, etc., properties to be evaluated after the first generation alloy was produced.

The experimentally measured conductivity of C77000 is $5.683 \% \pm 0.003 \% \text{ IACS}$, within the range reported in the available literature. Therefore the conductivity needed to be reduced by about 0.2 % IACS to meet the US Mint specification. Using the model described above, the calculated conductivity of C77000 is 5.52 % IACS, which was slightly lower than the experimentally measured value but still within the range reported in the available literature. The model was then used to determine how to adjust the conductivity by 0.2 % IACS, to 5.32 % IACS. The model predicted that the desired conductivity could be achieved by an increase in Ni-content of 0.01 mass fraction at the expense of Zn in the composition of C77000. Based on this composition, the first iteration of the modified C77000 alloy, C77D, was established with a composition of Cu-0.19Ni-0.26Zn-0.003Mn mass fraction.

C77D-2, the first 1 kg heat produced had an A-WQ conductivity of $5.524 \% \pm 0.056 \% \text{ IACS}$ and hardness of $(104.6 \pm 3.7) \text{ VHN100}$. Both values met the US Mint requirements. An additional five heats of C77D were produced, 2 kg of which were provided to the US Mint and the remaining material used for NIST characterization of tensile properties and corrosion behavior. Figure 11 presents the conductivity and hardness of the C77D alloys compared to C71300 and C77000 (C77D-7 was only used for mechanical and corrosion tests). Note that the 2 kg of material supplied to the US Mint were taken from the four heats C77D-3 through C77D-6. The conductivity and hardness values shown for these heats are the combined results provided by the US Mint, hence the large combined bar for these for heats.

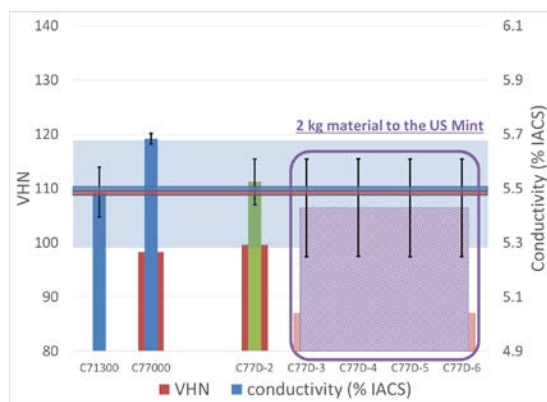


Figure 11: Conductivity and Vickers microhardness of C77D alloys, heats 2-6, compared to C71300 and C77000. Error bars represent the standard deviation of at least five measurements.

It should be noted that the error bars for these combined lots of material are roughly twice that for any other material. There are two main factors that could give rise to this variability in measured conductivity. First, the 2 kg was consisted of four separate melts, and the composition of these melts may vary slightly despite the best efforts to keep them identical. Second, and more likely, it the thickness control of the sheet produced at NIST. The laboratory scale rolling mill used at NIST is not designed to produce material with a uniform thickness within the tolerances required by the US Mint. Spot checks of sheet thickness suggested that the thickness was about $1.63 \text{ mm} \pm 0.051 \text{ mm}$; but the actual variation may have been larger. The eddy current method used to measure conductivity uses multiple frequencies between 60 kHz and 480 kHz. The penetration depth of the measurement varies as a function of the frequency (i.e., the lower the frequency the deeper the penetration depth). At 60 kHz, the penetration depth is greater than the thickness of the sheet (or coin,) so the measured conductivity is strongly influence by the thickness of the sample. Therefore at high frequencies (240 kHz or 480 kHz), the measured conductivity of C77D is a match with C71300; but at low frequencies, the variation in coin thickness altered the measurement to cause the observed scatter in conductivity measurements. Note that most coin acceptors perform a sweep over a set range in eddy current frequencies to assess the electric characteristics of the coins.

This variation in measured conductivity with sheet thickness was unforeseen, and in turn, caused some issues when the material was stamped into coins and tested by the US Mint. Multiple coin acceptor machines are used by the US Mint to evaluate the acceptance rate of coins. While 100 % of the coins produced were accepted using the in house unit at the US Mint, the acceptance rate measured by a vendor external to the US Mint with a tighter acceptance window was only about 70 %. Fortunately, both the possible variation in composition from heat to heat and the known variation in sheet thickness are easily mitigated when the production is scaled to a commercial level.

The discovery of the thickness dependence did reveal an important design consideration. The US Mint redesigned the dies to produce a slightly thicker coin because of the small difference in density between C71300 and the new prototype alloys being developed. While this change results in no observable different in the appearance of feel of the final coin, it allows a coin made from the new material to be identical in mass to those made with C71300. As a result of the

planned change in thickness, the conductivity of coins made of C77D measured at 240 kHz and 480 kHz was a match with C71300. However, when measured at 60 kHz, the conductivity of the C77D coins was about 0.2 % IACS above those made of C71300. This required a slight modification to the target conductivity of the new materials: Instead of exactly matching the electrical conductivity of C71300, the new alloys would exhibit a conductivity 0.1 % IACS less than that of C71300 at high frequency. As a result of the difference in thickness, the measured conductivity at low frequency would be 0.1 % IACS greater than C71300 for both the sheet and the coin. The resulting material would then meet the acceptor tolerances at both high and low sampling frequencies. This result prompted further conductivity measurements on the NIST material to be performed at 480 kHz rather than 240 kHz to ensure the elimination of thickness effects. The composition of C77D for patenting and scale-up was modified slightly to accommodate this new change in target conductivity, which will be discussed in the next section.

4.3.2. Mechanical properties

Figure 12 shows the representative true tensile stress-strain behavior of the C77D, the commercial C71300 and the C77000. Both the C77D and the C77000 are both significantly stronger and more ductile than the binary C71300. Similar mechanical properties were expected for C77D and C77000 as the compositions are similar. The slightly lower yield strength, ultimate tensile strength, and slightly higher ductility of C77D compared to the C77000 are most likely due to the presence of tramp impurities in the C77000 alloy. Both C77D and the C77000 met the mechanical properties requirements of the US Mint.

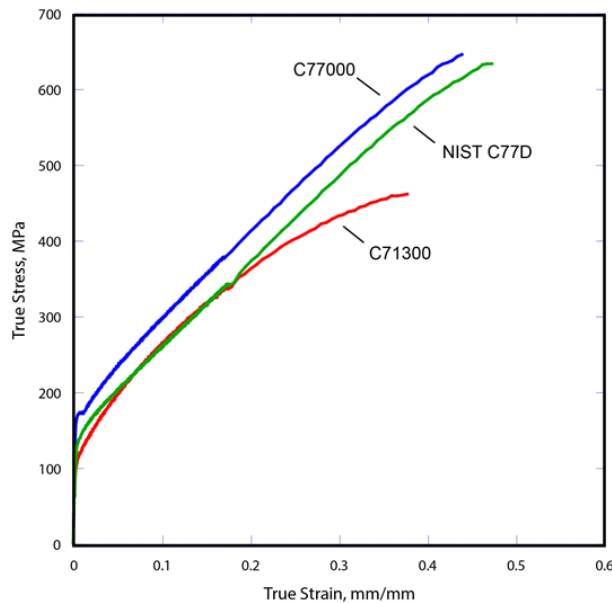


Figure 12: Representative tensile testing results of NIST C77D compared the commercial C71300 and C77000.

The results from the mechanical property analyses of C71300, C77000, and C77D are summarized in Table 5. The properties K and n are the work hardening coefficient and exponent, respectively, which are related to the true stress-strain curve by the following equation:

$$\sigma = K\varepsilon^n \quad (5)$$

On a log plot, these values are the intercept and slope of the true stress strain curve respectively. The K and n values were determined over two strain regions: from 0.01 to 0.1, and from 0.1 to 0.15. The former range defines the work hardening just beyond the yield, and is of particular interest to coin stamping processes. The second range denotes a region where the plastic flow (work hardening rate) has stabilized. Note the initial work hardening of C77D and C77000 are lower than C71300, which suggests that both these alloys may flow more easily than C71300 during the coining process.

Table 5: Summary of the measured mechanical properties of C71300, C77000, and NIST C77D. Note: a standard deviation of 0 indicates that the actual value is smaller than the range shown in the table.

Alloy	σ_y , MPa	σ_{UTS} , MPa	True Fracture Stress, MPa	Strain to Failure	K (0.01-0.1), MPa	n (0.01-0.1)	K (0.1-0.15), MPa	n (0.1-0.15)
C71300	113 ± 4	323 ± 2	463 ± 02	0.43 ± 0.01	650 ± 08	0.16 ± 0.00	739 ± 04	0.18 ± 0.01
C77000	164 ± 1	417 ± 1	645 ± 00	0.47 ± 0.02	572 ± 01	0.12 ± 0.00	922 ± 01	0.20 ± 0.00
C77D	129 ± 1	395 ± 3	627 ± 13	0.49 ± 0.01	511 ± 24	0.13 ± 0.01	898 ± 17	0.23 ± 0.00

4.3.3. Electrochemical behavior

The data in Figure 13a show that the C77000 achieves a steady-state FCP faster than the C71300 and the C77D alloys in the Na₂SO₄ solution. The results also indicate that the FCP of C77D was more cathodic (negative) to the other alloys in this solution. The FCP of C71300 binary alloy fluctuated more than the C77000 and the C77D alloys and did not reach an apparent steady-state potential after a 24 hour exposure. The behavior of the binary alloy was also substantially more anodic (positive) than the other alloys. This behavior suggests that active corrosion may be occurring, as this would tend to shift the potential toward that of the dominant reaction. The FCP behaviors in the simulated human sweat solution are shown in Figure 13b. The FCP for the C71300 was again significantly more anodic compared to the other alloys, but the alloy reached a steady-state potential in the sweat and did not indicate any active corrosion reactions. However, the composition of the simulated sweat solution is predominately distilled water with substantially less charge-carrying ions with respect to the sulfate solution, so the results may be more indicative of the lack of ionic species in this solution than an indication of the actual performance in service.

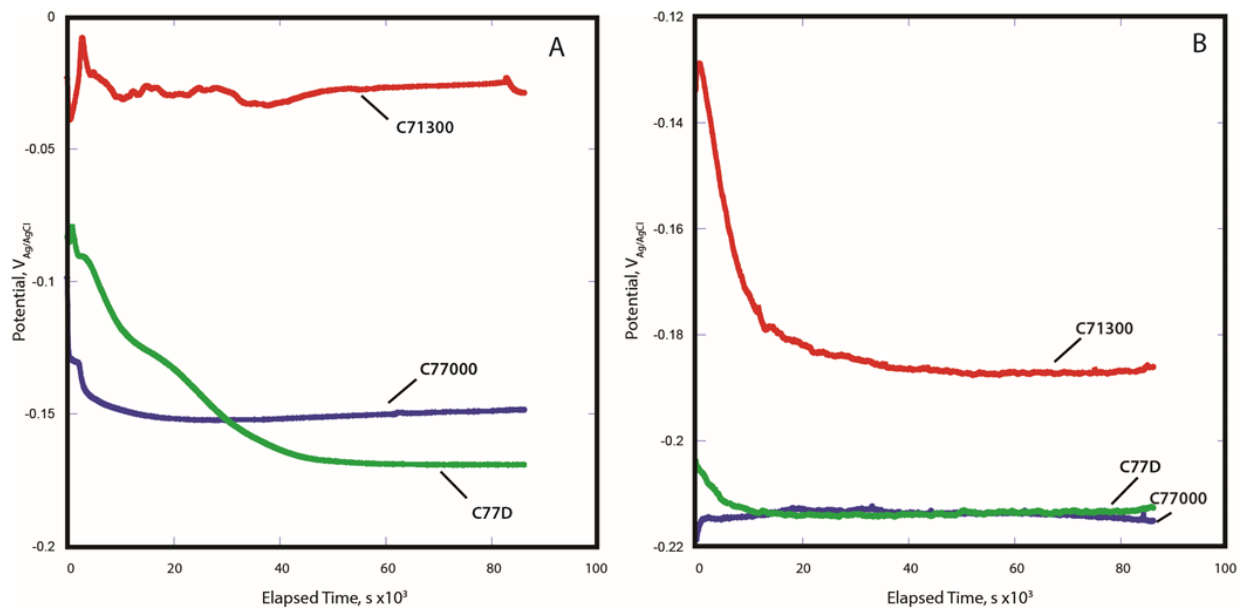


Figure 13: Comparison of C71300, C77000, and NIST C77D performance under free corrosion conditions in a) deaerated 0.5M Na_2SO_4 , and b) deaerated simulated human sweat solution.

Further analyses of the surfaces after the 24 hour exposures revealed that sulfate solution attacked the C71300, the C77000 and C77D alloys. Because all of these alloys contain a substantial fraction of zinc, they are particularly susceptible to selective dissolution (dealloying) where the zinc is dissolved preferentially to the other elements. Figure 14a shows significant pitting on the surface of the C71300. The pitting is evenly distributed along the surface, which could suggest that the dealloying (and therefore the zinc) was evenly distributed along the surface. In contrast, the attack on the surfaces of the C77000 (Figure 14b) and the C77D (Figure 14c) was significantly more localized. This could be an indication of an inhomogeneous microstructure or that there was a zinc-rich region in a preferential location to a pit or to other surface anomaly. The attack observed on the surface of the C77D is a classic illustration of how dealloying occurs in a brass-like alloy. Dealloying was generally not observed on the surface of any alloy in the sweat solution. Figure 13d through Figure 14f are representative of micrographs showing the surfaces after a 24 hour exposure in the deaerated sweat solution. Some attack is observable, but it is substantially less than what was observed in the sulfate.

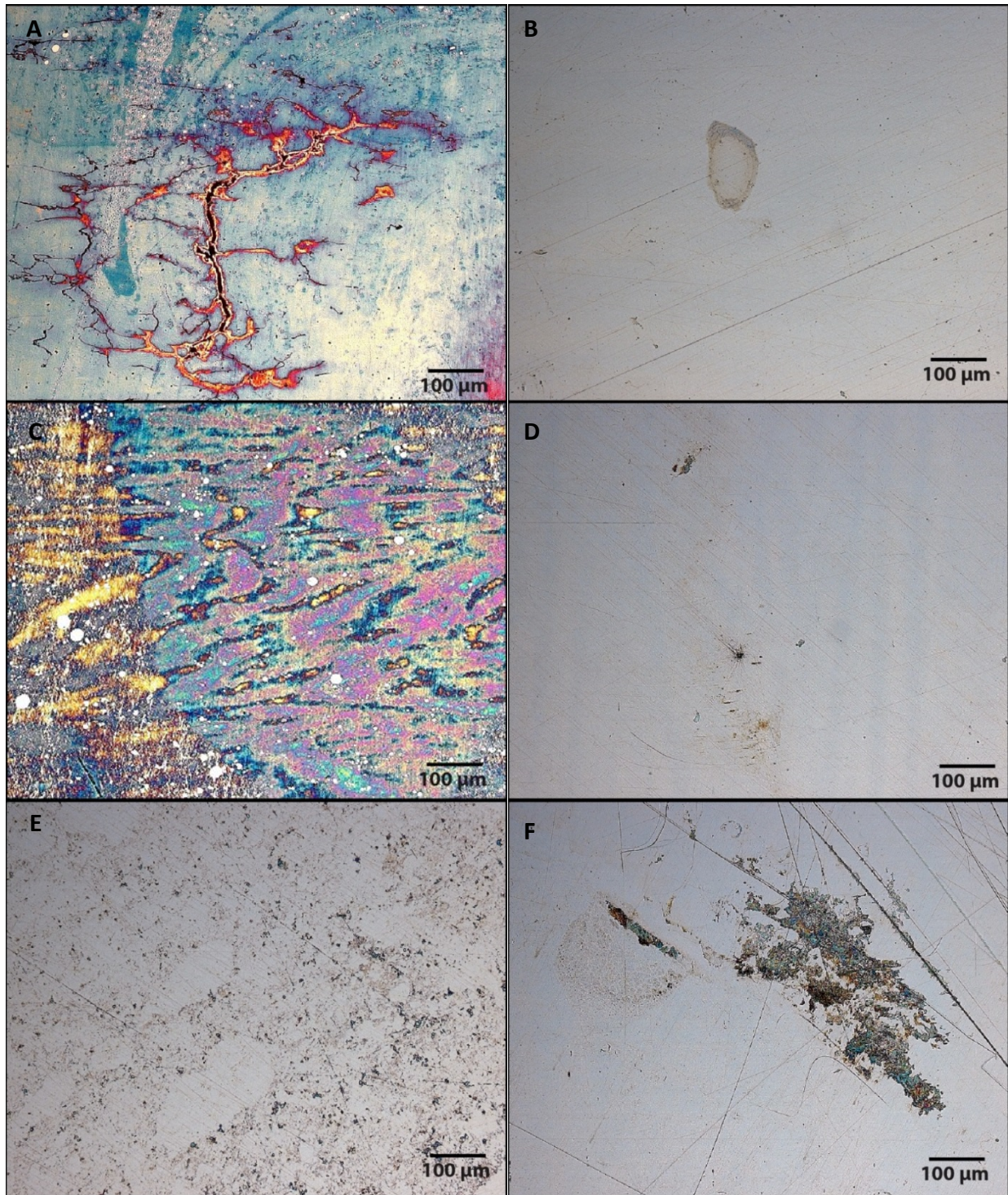


Figure 14: Optical micrographs of the C71300, C77000 and C77D alloys after a 24 hour exposure in deaerated 0.5M Na₂SO₄, and in deaerated simulated human sweat solution: a) and d), C71300 in sulfate and sweat respectively, b) and e), C77000 in sulfate and sweat respectively, and c) and f), C77D in sulfate and sweat respectively.

The dealloyed surface of the C77D was examined in the SEM. Figure 15 shows representative micrographs from that analysis. Figure 15a exhibits areas where the zinc-rich phase was

selectively dissolved creating a sponge-like appearance. A higher magnification view of the dealloyed region is shown in Figure 15*b*.

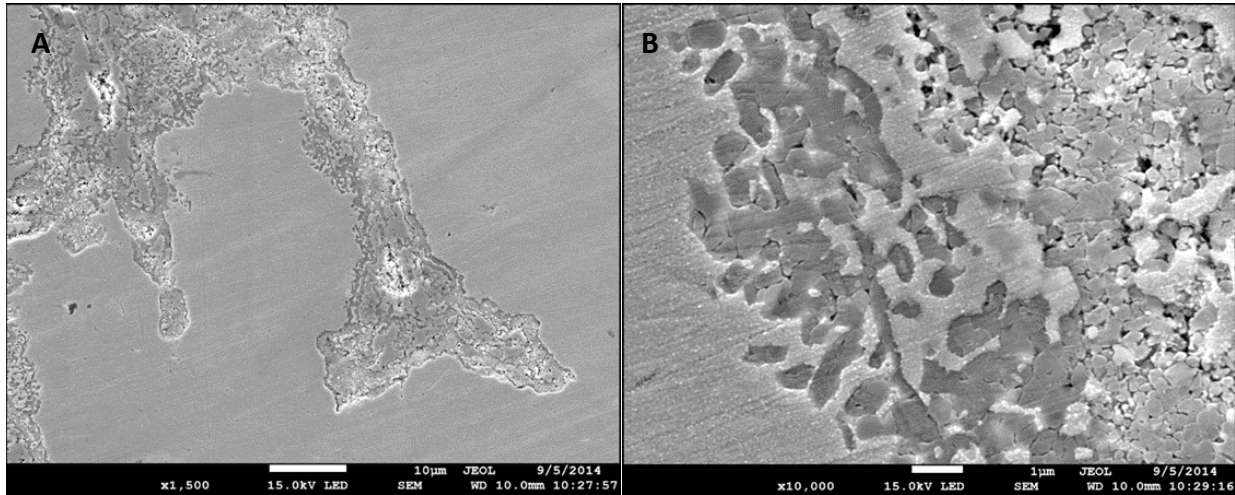


Figure 15: SEM micrographs of Zn de-alloying in C77D in the sulfate solution.

The performance of each alloy in the two solutions is presented in Figure 16. The figures are the electrode potential shown as a function of the log of the current. In thermodynamic terms, the potential is the thermodynamic driving force for a particular corrosion reaction, and the current is the rate at which that reaction occurs. As shown in Figure 16*a*, the behaviors of the C77000 and C77D alloys were quite similar in the sulfate solution whereas the behavior of the C71300 binary was slightly more anodic. All three alloys exhibited a relatively stable region of passivity in the sulfate solution and the onset of pitting occurred at approximately 0.000 V wrt Ag/AgCl. In the simulated sweat solution (Figure 16*b*), the behaviors of the three alloys were markedly different. While the overall trend was similar for the three alloys, the shift toward the higher current in the C77000 alloy indicates this alloy may be more active (i.e., corrodes faster) than the C71300 and the C77D. None of the alloys exhibited a particularly strong passive region, which suggests that pitting may occur almost immediately with an anodic current. As was the case for the FCP measurements, the results may be more indicative of the lack of ionic species in this solution than an indication of the performance in service.

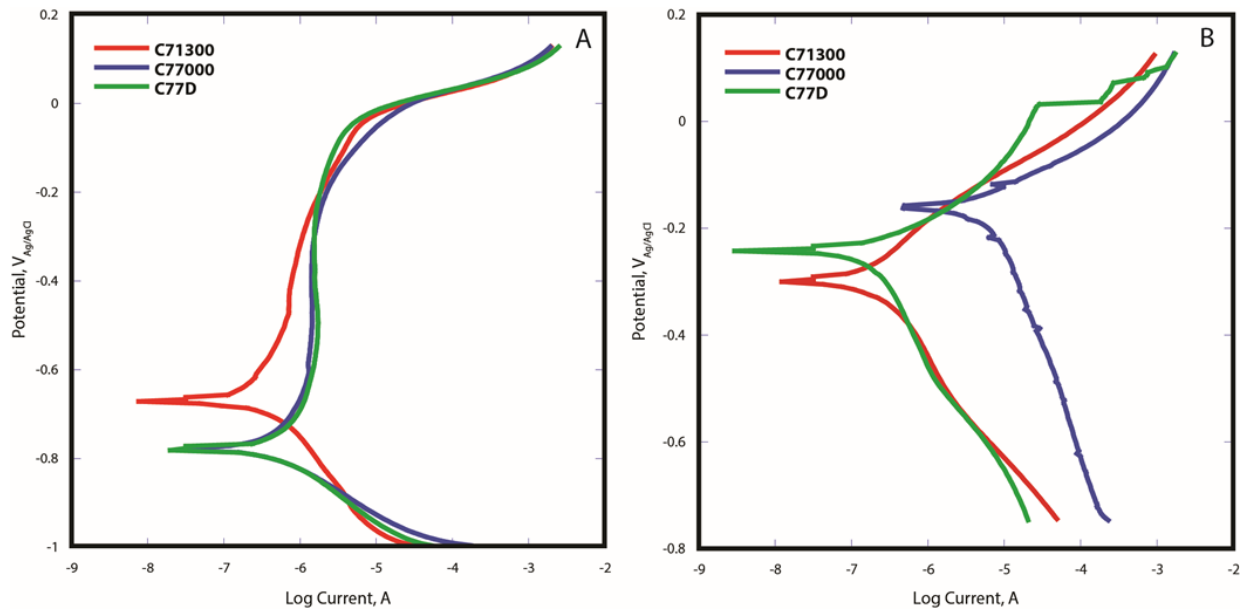


Figure 16: Comparison of the alloy performance using polarization resistance in a) deaerated 0.5M Na₂SO₄ and b) deaerated simulated human sweat solution.

4.3.4. US Mint characterized properties

The 2 kg of C77D provided to the US Mint by NIST was used to produce a lot of test coins for further characterization. The mechanical load required to stamp coins produced with C77D is actually lower than that required for C71300 by 5 % to 10 %. This is likely a result of the lower initial work hardening rate of C77D compared to C71300. The strength and work hardening rate of C77D is likely to increase slightly when the alloy is up-scaled to commercial levels due to the increased influence of impurities; but this increase should not be significant enough to cause issues with the use of this alloy as a potential replacement for C71300.

The results of the wear corrosion testing performed on C77D, C99R, and C71300 by the US Mint are summarized in Table 6. The wear resistance of C77D is considered excellent, as it is more than three times greater than C71300. In addition, the mass loss for C77D during week two is less than half that for week one and it is about 80 % of that for C71300. These results indicate that the wear resistance is significantly improved over the C71300.

Table 6: Results of the US Mint wear-corrosion testing of C77D and C99R, along with those of C71300 for comparison.

Alloy	Mass Loss-week one (%)	Mass Loss - week two (%)	Total Mass loss (%)
C71300	0.250 ± 0.014	0.207 ± 0.027	0.445 ± 0.019
C77D	0.086 ± 0.012	0.036 ± 0.008	0.122 ± 0.019
C99R	0.069 ± 0.020	0.016 ± 0.010	0.088 ± 0.016

4.4. Final Optimization of C77D'

As demonstrated by the above data, the C77D alloy meets all the requirements established by the US Mint. The experimentally measured composition of C77D (the average of all five heats) was Cu-0.193Ni-0.262Zn-0.003Mn mass fraction, which is slightly different than the nominal composition of Cu-0.19Ni-0.26Zn-0.003Mn mass fraction. The composition limits for Ni, Zn, Mn, and Fe were also determined to ensure the conductivity would be maintained within a ± 0.2 % IACS tolerance,. The effects of Fe were determined experimentally by producing alloy C77F, with a nominal composition identical to C77D except that 0.0025 mass fraction Fe was included at the expense of Cu. The conductivity of A-WQ C77F-1 was 5.409 ± 0.031 % IACS, suggesting that 0.0025 mass fraction Fe reduces the conductivity by approximately 0.1 % IACS.

The composition limits for Ni, Zn, and Mn were determined using the constructed conductivity model. Figure 17 presents the change of calculated conductivity with Ni and Zn compositions for four different Mn compositions, between 0.001 mass fraction and 0.005 mass fraction, and for three different mass fractions of Zn 0.24, 0.26, and 0.28. The plots illustrate the deviation in conductivity from the value calculated for the measures composition of C77D, 5.25 % IACS, up to ± 0.2 % IACS. The first observation is that Zn-content has little effect on conductivity, as expected. Looking at the conductivity change with Ni content, with 0.001 mass fraction of Mn the conductivity varies by less ± 0.2 % IACS for Ni compositions in the range of about 0.19 to 0.215 mass fraction Ni. At a 0.005 mass fraction of Mn, Ni composition range changes to 0.175 to 0.20 mass fraction Ni.

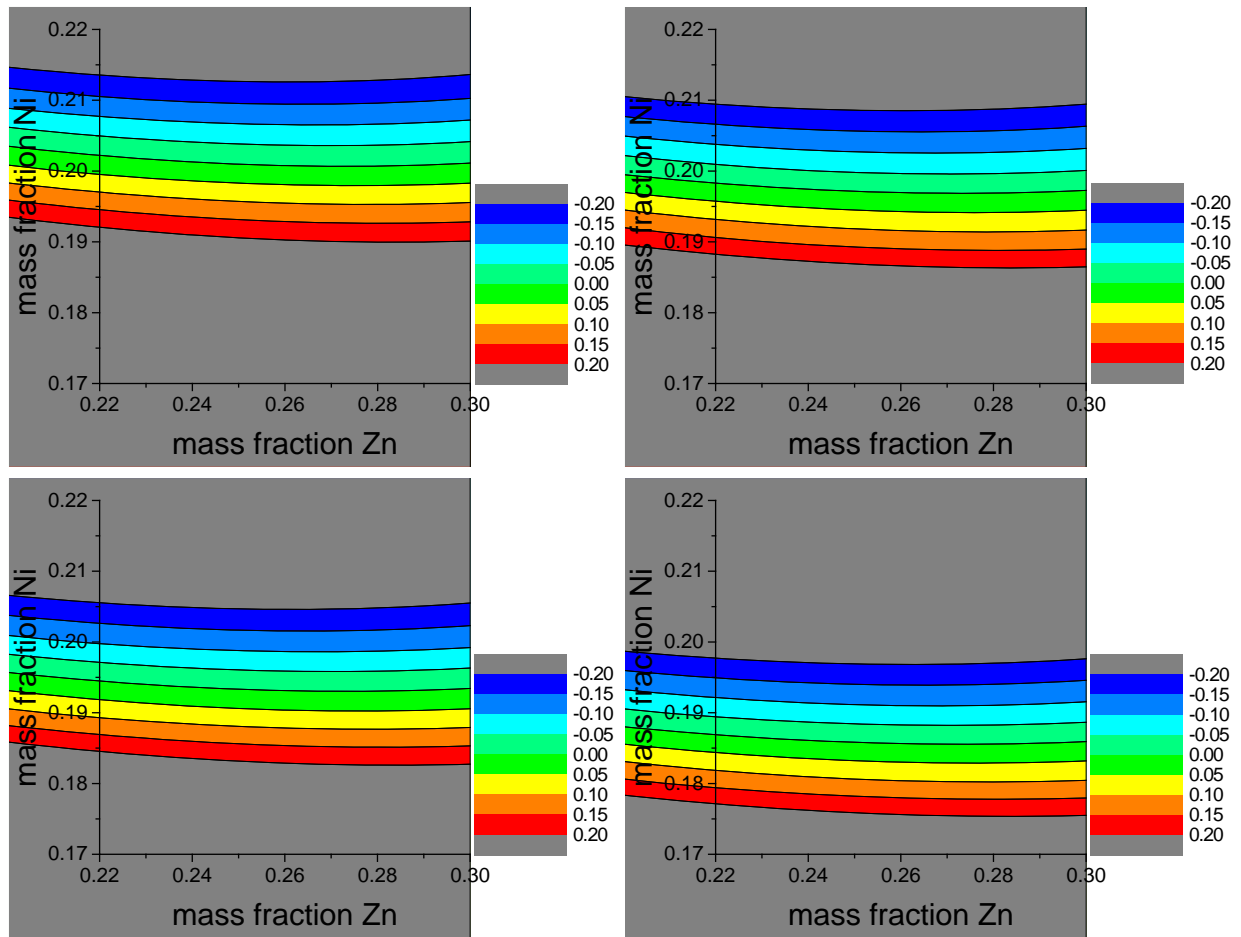


Figure 17: Calculated dependence on composition of the deviation in conductivity (± 0.2 % IACS) from the value calculated for the composition of C77D of 5.26 % IACS in quaternary Cu-Ni-Zn-Mn for Mn compositions of a) 0.001 mass fraction, b) 0.002 mass fraction, c) 0.003 mass fraction, and d) 0.005 mass fraction, and for Zn compositions of e) 0.24 mass fraction, f) 0.26 mass fraction and g) 0.28 mass fraction.

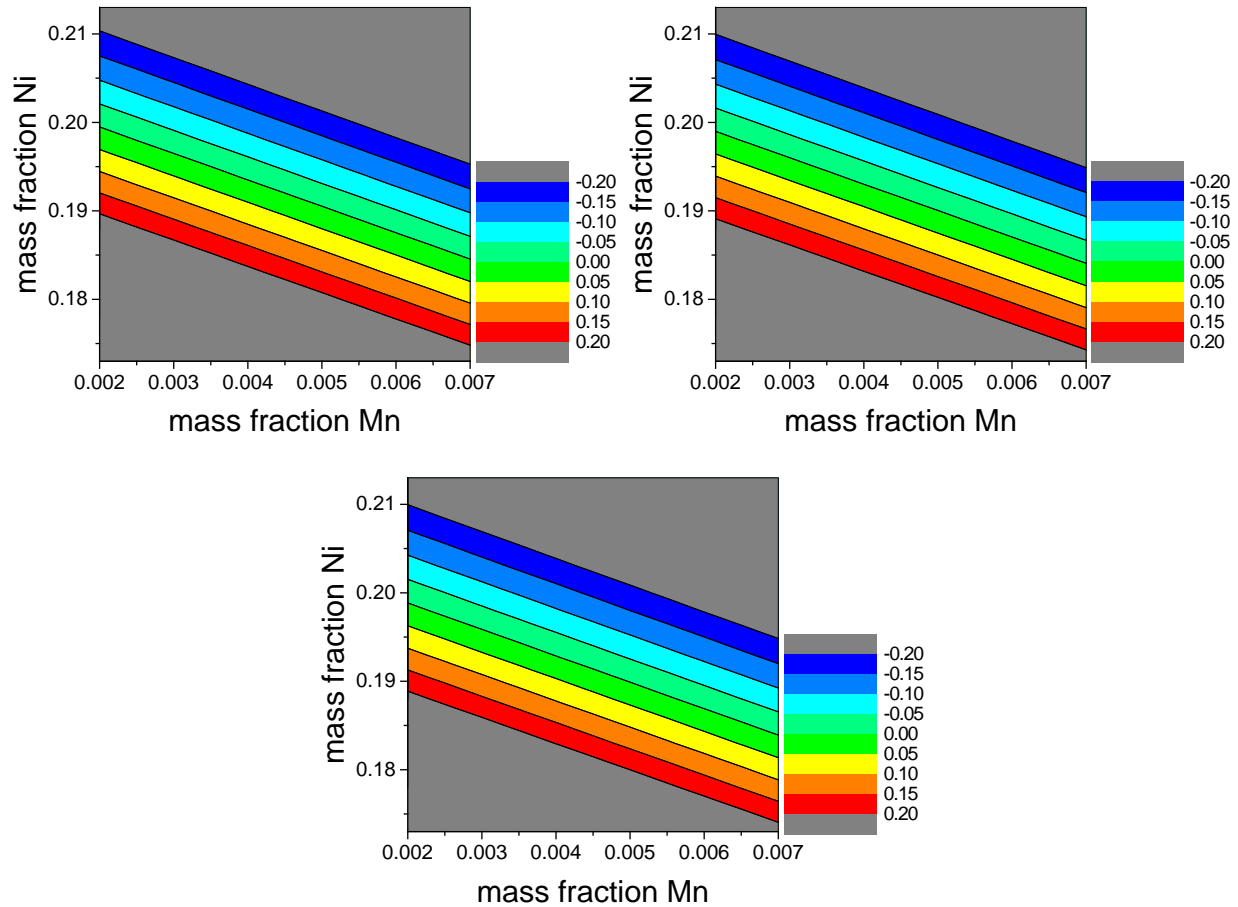


Figure 17 (cont.): Calculated dependence on composition of the deviation in conductivity (± 0.2 % IACS) from the value calculated for the composition of C77D of 5.26 % IACS in quaternary Cu-Ni-Zn-Mn for Mn compositions of a) 0.001 mass fraction, b) 0.002 mass fraction, c) 0.003 mass fraction, and d) 0.005 mass fraction, and for Zn compositions of e) 0.24 mass fraction, f) 0.26 mass fraction and g) 0.28 mass fraction.

Using the experimental results of C77F-1 and the calculated the data, two extreme compositions were determined, C77G and C77H in Table 7. The two alloys were then produced and their conductivity measured. The conductivities of C77G-1 and C77H-1 were 5.221 % \pm 0.037 % IACS and 5.754 % \pm 0.039 % IACS, respectively, or about 0.25 % below and above the 5.524 % \pm 0.056 % IACS measured for C77D-2. To further tighten the conductivity range, The Ni tolerance range was refined from the predicted range of 0.18 to 0.20 mass fraction Ni to range of 0.182 to 0.198 mass fraction Ni.

Table 7: Final composition of the NIST modified C77000 alloy, C77D', compared to that of commercial C77000 and C77D. Nominal compositions are in parentheses. Note all compositions are given in mass fractions $\times 100$.

Alloy	Cu	Ni	Zn	Mn	Fe	Pb
C77000	53.5 to 56.5 (55)	16.5 to 19.5 (18)	Bal. (27)	<0.5	<0.25	<0.05
C77D	Bal.	18.2 to 19.8 (19.0)	24.0 to 28.0 (26.0)	0.2 to 0.5 (0.3)	<0.2	N/A
C77D'	Bal.	18.5 to 20.1 (19.3)	24.0 to 28.0 (26.0)	0.3 to 0.6 (0.4)	<0.2	N/A

One additional modification needed to be made to C77D before it was finalized. As a result of the issue influence of thickness on the conductivity signatures measured by the vending machines (section 4.3.1), the target conductivity was reduced by about 0.1 % IACS from 5.45 % IACS to 5.35 % IACS. Using the conductivity model, the alloy composition was re-optimized to increase the nominal Ni-content from 0.190 mass fraction to 0.193 mass fraction (the C77D measured composition) and increase the nominal Mn-content from 0.003 mass fraction to 0.004 mass fraction to meet the target conductivity objectives. New tolerances were determined that were based on this refined prototype composition and is noted as C77D'. The C77D' composition has been chosen to begin the up-scaling to a commercial production process with US Mint materials supplies. A patent is also being pursued for this alloy and the processing conditions required to obtain the desired properties. Note that the alloy was designed to match the specific processing condition used by the US Mint, which include a specified annealing treatment followed by a water quench. As NIST C77D' is designed using explicit processing conditions to achieve specific material properties, the alloy composition constitute a patentable invention, despite the composition being similar to the commercial C77000. Figure 18 is the finalized alloy data sheet for NIST C77D'.

NIST C77D' Alloy Data Sheet

- Composition:

Cu	Ni (19.3 %)	Zn (26.0 %)	Mn (0.4 %)	Fe (0 %)
Bal.	18.5 to 20.1	24.0 to 28.0	0.3 to 0.6	<0.2

- Conductivity (annealed 700 °C to 800 °C, 30 min, water quench): 5.4±0.2 % IACS
- Mechanical Properties (annealed):
 - Yield strength: 145±20 MPa
 - Strain to failure: >50 %
 - Work-hardening exponent: 0.13 ($\epsilon=0.01$ to 0.1), 0.23 ($\epsilon=0.1$ to 0.15)
 - Wear-resistance: 3x greater than C71300
- Color: as white or better than C71300 (no red)
- Corrosion:
 - US Mint steam test: passed
 - US Mint wear test: passed
 - NIST electrochemical testing (sweat): no significant attack
 - NIST electrochemical testing (sodium sulfate): localized attack, Zn dealloying
- Cost: about 20 % less than C71300, based on material costs
- Additional notes:
 - This alloy has been designed to exhibit the above properties when annealed at 700 °C to 800 °C for 30±10 min and water quenched. Thermal processing outside of the prescribed range may result in properties that deviate from those outlined above

Figure 18: NIST C77D' alloy data sheet. Note the compositions listed are in mass fractions multiplied by 100

5. Alloy design of C99-series alloys

5.1. Test alloys

The conductivity data in Table 2 for commercial alloys was insufficient for constructing and calibrating a composition dependent model of conductivity for alloys with significant Mn-content. A series of four test alloys were produced to supplement the limited conductivity data, and were labeled as C99A-1, C99B-1, C99C-1, and C99D-1, and the nominal compositions follow the formula, (given in mass fractions multiplied by 100) were Cu-5Ni-(40- x)Zn- x Mn, where x equals, 10, 15, 20, and 25, respectively. The test alloys were later expanded to include C99E-1 and C99E-2, where x equals 5 for both, but different amounts of extra Zn were added to offset Zn evaporation losses. A ternary alloy Cu-40Zn-7Mn, C99F-1, was also produced to investigate the properties of a β single-phase alloy. The conductivity of the β phase was found to be greater than that of the α -fcc phase; however the microhardness was found to be too high and the color was much too yellow for coinage applications. The measured properties of these alloys and the alloys produced during the C99 series alloy development are summarized in Table 8.

Table 8: Summary of alloys produced during the development of the C99 series alloys. All alloy compositions are given in mass fractions multiplied by 100. Notes: a) added 0.20 mass fraction Zn, 0.04 mass fraction Cu, and 0.15 mass fraction Mn extra, b) added 0.10 mass fraction Zn, 0.04 mass fraction Cu, and 0.15 mass fraction Mn extra, c) added mass fraction of Zn and 0.15 mass fraction Mn extra, d) added 0.15 mass fraction Zn and 0.15 mass fraction Mn extra, e) added 0.10 mass fraction Zn and Mn extra, f) added 0.125 mass fraction of Zn and 0.10 mass fraction Mn extra, g) added 0.125 mass fraction Zn and Mn extra, h) surface milled prior to rolling. Condition legend: AC-as cast; CR-cold rolled; WR-warm (hot) rolled; A-annealed; WQ-water quenched. The ingot mass is in grams.

Date	Designation (condition)	Nominal Composition (mass fraction time 100)	Mass (g)	Comments	Measured Composition				Conductivity 240 kHz (IACS)	Hardness VHN100 (kg/mm ²)	L	Color	
					Ni	Zn	Mn					a	b
N/A	C71300 (in use)	Cu-25Ni-0.3Mn			25.77±0.27		0.33±0.05		5.472±0.100	78.3±1.3	1.04±0.06	5.29±0.29	
7/9/2014	C99A-1 (AC)	Cu-5Ni-30Zn-10Mn	200		5.45±0.08	27.56±0.18	9.28±0.14		3.537±0.021				
	C99A-1 (CR)								243.4±5.7				
	C99A-1 (CR-A-WQ)								94.5±3.1	82.4±0.2	0.04±0.04	7.52±0.12	
7/9/2014	C99B-1 (AC)	Cu-5Ni-25Zn-15Mn	200		5.64±0.07	20.98±0.13	14.32±0.08		2.654±0.033				
	C99B-1 (CR)								250.0±6.8				
	C99B-1 (CR-A-WQ)								101.1±3.5	79.9±1.3	0.26±0.02	5.48±0.24	
7/9/2014	C99C-1 (AC)	Cu-5Ni-20Zn-20Mn	200		5.47±0.11	17.51±0.17	18.80±0.16		2.187±0.009				
	C99C-1 (CR)								250.1±8.6				
	C99C-1 (CR-A-WQ)								108.5±4.3	78.8±0.5	0.41±0.02	4.49±0.24	
7/9/2014	C99D-1 (AC)	Cu-5Ni-15Zn-25Mn	200		5.58±0.08	12.28±0.15	23.63±0.08		1.867±0.022				
	C99D-1 (CR)								253.8±8.8				
	C99D-1 (CR-A-WQ)								121.4±2.8	77.1±0.7	0.62±0.05	3.43±0.42	
7/24/2014	C99E-1 (AC)	Cu-5Ni-35Zn-5Mn	200	a	4.78±0.10	38.32±0.11	4.64±0.14		5.836±0.070				
	C99E-1 (CR)								248.6±6.7				
	C99E-1 (CR-A-WQ)								135.4±8.2	82.5±0.7	0.23±0.04	9.76±0.53	
7/24/2014	C99F-1 (AC)	Cu-40Zn-7Mn	200	a					10.057±0.119				
	C99F-1 (WR)								239.6±11.3				
	C99F-1 (WR-A-WQ)					44.76±0.13	6.25±0.21		6.946±0.165	82.4±0.8	0.94±0.06	10.96±0.25	
8/11/2014	C99B-2 (AC)	Cu-5Ni-25Zn-15Mn	1000		4.82±0.10	25.60±0.12	13.44±0.18						
	C99B-2 (WR)								244.6±5.1				
	C99B-2 (WR-A-WQ)								98.7±3.6	79.2±2.3	-0.34±0.22	11.30±1.45	
8/11/2014	C99E-2 (AC)	Cu-5Ni-35Zn-5Mn	200	b	4.55±0.06	35.04±0.15	5.05±0.07		5.493±0.022				
	C99E-2 (WR)								4.934±0.003				
	C99E-2 (WR-A-WQ)								5.280±0.010	84.79±1.7	0.35±0.19	6.65±0.37	

Table 8 (cont.): Summary of alloys produced during the development of the C99 series alloys. All alloy compositions are given in mass fractions multiplied by 100. Notes: a) added 0.20 mass fraction Zn, 0.04 mass fraction Cu, and 0.15 mass fraction Mn extra, b) added 0.10 mass fraction Zn, 0.04 mass fraction Cu, and 0.15 mass fraction Mn extra, c) added mass fraction of Zn and 0.15 mass fraction Mn extra, d) added 0.15 mass fraction Zn and 0.15 mass fraction Mn extra, e) added 0.10 mass fraction Zn and Mn extra, f) added 0.125 mass fraction of Zn and 0.10 mass fraction Mn extra, g) added 0.125 mass fraction Zn and Mn extra, h) surface milled prior to rolling. Condition legend: AC-as cast; CR-cold rolled; WR-warm (hot) rolled; A-annealed; WQ-water quenched. The ingot mass is in grams.

Date	Designation (condition)	Nominal Composition (mass fraction time 100)	Mass (g)	Comments	Measured Composition			Conductivity 240 kHz (IACS)	Hardness VHN100 (kg/mm ²)	L	Color	
					Ni	Zn	Mn				a	b
8/29/2014	C99G-2 (AC)	Cu-7Ni-33.5Zn-4.5Mn	200	c	7.54±0.16	30.88±0.16	4.60±0.11	5.272±0.009		84.7±0.7	-0.32±0.04	9.45±0.15
	C99G-2 (WR)						5.137±0.013					
	C99G-2 (WR-A-WQ)						5.295±0.023					
9/17/2014	C99H-1 (WR)	Cu-6Ni-25Zn-14Mn	1000		6.22±0.11	23.83±0.33	14.37±0.22		153.9±4.8			
	C99H-1 (WR-A-WQ)						2.514±0.009 ^f	102.6±4.1	80.4±1.3	0.15±0.01	5.15±0.10	
9/24/2014	C99I-2 (WR)	Cu-11Ni-26Zn-3Mn	200	d	11.23±0.19	26.81±0.30	3.04±0.06			81.2±0.1	-0.25±0.08	7.94±0.41
	C99I-2 (WR-A-WQ)						5.640±0.027 ^f					
9/24/2014	C99J-1 (WR)	Cu-14Ni-29Zn-2Mn	200	d	14.20±0.20	29.39±0.26	2.04±0.06					
	C99J-1 (WR-A-WQ)						5.457±0.007 ^f		83.0±0.3	-0.51±0.05	7.35±0.08	
10/7/2014	C99K-1 (WR)	Cu-9Ni-30Zn-3.5Mn	200	e	9.47±0.16	28.69±0.28	3.50±0.05					
	C99K-1 (WR-A-WQ)						5.643±0.007 ^f		83.5±0.8	-0.29±0.05	9.10±0.28	
11/10/2014	C99L-1 (WR)	Cu-11Ni-23Zn-3.5Mn	200	f	11.15±0.11	23.87±0.25	3.40±0.05					
	C99L-1 (WR-A-WQ)						5.523±0.012 ^f		83.1±1.1	-0.05±0.03	8.25±0.28	
11/10/2014	C99M-1 (WR)	Cu-13.5Ni-26Zn-2.5Mn	200	f	14.06±0.31	23.04±0.84	2.43±0.07					
	C99M-1 (WR-A-WQ)						5.447±0.022 ^f		82.1±1.4	-0.36±0.06	7.38±0.21	
11/10/2014	C99N-1 (WR)	Cu-5Ni-21Zn-5.5Mn	200	f	5.23±0.13	20.30±0.23	5.39±0.09					
	C99N-1 (WR-A-WQ)						5.472±0.015 ^f		83.7±1.1	0.71±0.23	10.24±0.21	
12/11/2014	C99H-3 (WR)	Cu-6Ni-25Zn-14Mn	1000		6.25±0.07	24.77±0.16	12.72±0.05		217.0±11.5			
	C99H-3 (WR-A-WQ)						2.821±0.007 ^f	95.3±3.0				
12/29/2014	C99H-4 (WR)	Cu-6Ni-25Zn-14Mn	1000		6.21±0.08	25.53±0.14	12.59±0.06		218.9±9.5			
	C99H-4 (WR-A-WQ)						2.851±0.008 ^f	93.6±1.0				
12/30/2014	C99O-1 (WR)	Cu-14Ni-28Zn-3Mn	1000		14.64±0.21	27.16±0.34	2.72±0.06		211.4±10.8			
	C99O-1 (WR-A-WQ)						5.130±0.013 ^f	93.3±3.3	84.3±0.9	-0.40±0.05	7.44±0.13	

Table 8 (cont.): Summary of alloys produced during the development of the C99 series alloys. All alloy compositions are given in mass fractions multiplied by 100. Notes: a) added 0.20 mass fraction Zn, 0.04 mass fraction Cu, and 0.15 mass fraction Mn extra, b) added 0.10 mass fraction Zn, 0.04 mass fraction Cu, and 0.15 mass fraction Mn extra, c) added mass fraction of Zn and 0.15 mass fraction Mn extra, d) added 0.15 mass fraction Zn and 0.15 mass fraction Mn extra, e) added 0.10 mass fraction Zn and Mn extra, f) added 0.125 mass fraction of Zn and 0.10 mass fraction Mn extra, g) added 0.125 mass fraction Zn and Mn extra, h) surface milled prior to rolling. Condition legend: AC-as cast; CR-cold rolled; WR-warm (hot) rolled; A-annealed; WQ-water quenched. The ingot mass is in grams.

Date	Designation (condition)	Nominal Composition (mass fraction time 100)	Mass (g)	Comments	Measured Composition			Conductivity 240 kHz (IACS)	Hardness VHN100 (kg/mm ²)	L	Color	
					Ni	Zn	Mn				a	b
12/30/2014	C99P-1 (WR) C99P-1 (WR-A-WQ)	Cu-7.5Ni-25Zn-4.5Mn	200	g	7.99±0.11	22.54±0.19	4.55±0.07	5.313±0.015' 5.336±0.008'	199.8±10.2 90.3±3.1	83.0±1.1	0.40±0.08	9.99±0.34
12/30/2014	C99Q-1 (WR) C99Q-1 (WR-A-WQ)	Cu-10Ni-25Zn-4Mn	200	g	10.58±0.23	24.02±0.28	3.94±0.06	5.212±0.015' 5.337±0.012'	201.2±11.6 92.9±2.4	84.0±1.0	0.13±0.15	8.97±0.55
1/9/2015	C99H-5 (WR) C99H-5 (WR-A-WQ)	Cu-6Ni-25Zn-14Mn	1000	h	6.27±0.12	24.92±0.27	12.68±0.07	2.683±0.007'				
1/9/2015	C99H-6 (WR) C99H-6 (WR-A-WQ)	Cu-6Ni-25Zn-14Mn	1000	h	6.25±0.11	24.98±0.15	12.78±0.07	2.689±0.023'				
1/20/2015	C99R-1 (WR) C99R-1 (WR-A-WQ)	Cu-14Ni-28.5Zn-2.5Mn	1000		14.42±0.21	28.20±0.15	2.22±0.04	5.374±0.011'				
2/5/2015	C99R-2 (WR) C99R-2 (WR-A-WQ)	Cu-14Ni-28.5Zn-2.5Mn	1000	h	14.20±0.13	27.20±0.51	2.43±0.04					
2/11/2015	C99R-3 (WR) C99R-3 (WR-A-WQ)	Cu-14Ni-28.5Zn-2.5Mn	1000	h	14.53±0.09	28.14±0.18	2.27±0.06					
2/11/2015	C99R-4 (WR) C99R-4 (WR-A-WQ)	Cu-14Ni-28.5Zn-2.5Mn	1000	h	14.68±0.17	28.23±0.35	2.26±0.04					
2/11/2015	C99R-5 (WR) C99R-5 (WR-A-WQ)	Cu-14Ni-28.5Zn-2.5Mn	1000	h	14.40±0.07	28.23±0.24	2.28±0.03					
3/9/2015	C99H-8 (WR) C99H-8 (WR-A-WQ)	Cu-6Ni-25Zn-14Mn	1000	h	6.19±0.08	23.24±0.11	14.11±0.08					
3/11/2015	C99H-9 (WR) C99H-9 (WR-A-WQ)	Cu-6Ni-25Zn-14Mn	1000	h	6.10±0.10	23.89±0.23	13.97±0.18					

Figure 19 presents the measured electrical conductivities and Vickers microhardness values of the test alloys C99A-1 through C99E-2 in the A-WQ condition. For alloys C99A through C99D, the Mn-content is increased at the expense of Zn, the electrical conductivity decreases and the hardness increases. Above approximately 0.20 mass fraction Mn, the hardness surpasses the specified requirement of the US Mint. This adds an additional design constraint on the Mn composition for these alloys. At 0.10 mass fraction Mn (C99A), the hardness is sufficiently low but the conductivity is only $3.550 \pm 0.043 \%$ IACS. Also note in Table 8 that the yellowness value b^* continuously increases with decreasing Mn-content, and by C99A-1 b^* is at 7.52 ± 0.12 .

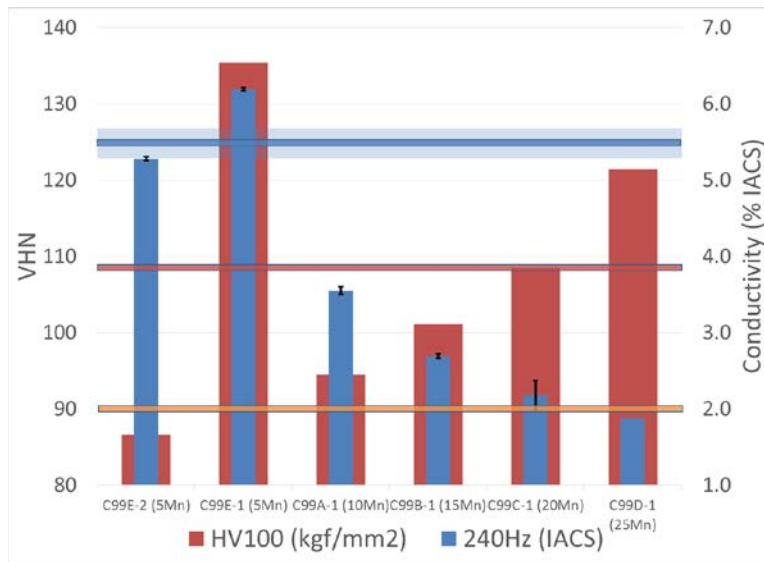


Figure 19: Measured electrical conductivities and Vickers microhardness values for C99 test alloys (C99F-1 not included) in the annealed and water quenched condition. Error bars represent the standard deviation of at least five measurements.

Significant jumps in both conductivity and hardness are observed for alloy C99E-1 when the concentration of Mn is decreased to 0.05 mass fraction. This is due to the formation of the β -bcc phase, which can be seen in Figure 20a. The microstructure of C99E consists of a nearly equal amount of α -fcc and β -bcc phases. The bcc phase can be seen as the darker colored grains in the figure. This phase is harder and higher in conductivity, thus producing the observed increases in Figure 19. The C99E-2 alloy differs from C99E-1 in that only 0.10 mass fraction extra Zn was added to offset Zn evaporation compared to 0.20 mass fraction extra Zn in C99E-1. This resulted in a decrease in the final Zn concentration from 0.382 mass fraction in C99E-1 to 0.35 mass fraction in C99E-2. This decrease in Zn-content reduced the phase fraction for the bcc phase from almost 0.5 to only approximately 0.02, which was found along grain boundaries, (this can be seen in Figure 20b). As the fcc phase is still the majority phase in C99E-2, the measured conductivity and hardness continue the trend observed in C99A through C99D alloys. C99E-2 has the lowest hardness of the test alloys. The conductivity is slightly lower than the required value for the monolithic C99 series alloy, and the yellowness is less than 7. Since this alloy shows the presence of the bcc phase, and the uncertainty that it brings to the final microstructure after processing, the C99E-2 is not acceptable for the US Mint's purposes. An alloy with a 100 % fcc microstructure is desired.

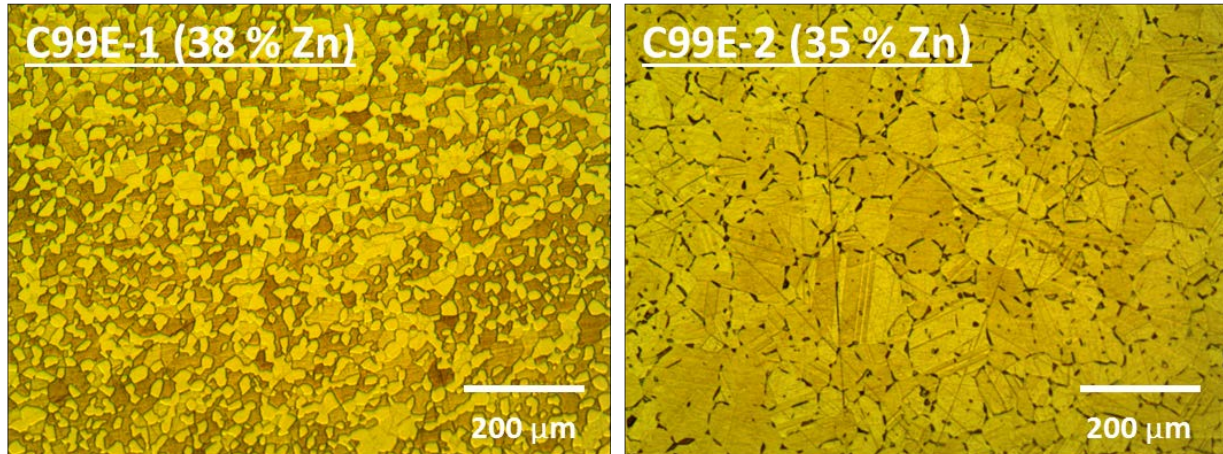


Figure 20: Micrographs of the two-phase microstructures found in C99E-1 and C99E-2. In addition to α -fcc, β -bcc phase is also observed as darker grains in C99E-1 and as dark precipitates along grain boundaries in C99E-2.

The calculated phase diagrams in Figure 3 suggest that the phase boundary between single-phase fcc and two-phase fcc+bcc is about 0.03 mass fraction Ni (for 0.55 mass fraction Cu) at zero fraction Mn, and that the solubility of Ni decreases with increasing Mn-content. The presence of bcc in C99E-1 and C99E-2 confirm that the calculated boundary is incorrect. Therefore, the compositions of the bcc and fcc phases in C99E-1 were measured to provide phase boundary information to further guide the alloy development process. The measured composition of the fcc and bcc phases are given in Table 9. These results show that the minimum Ni concentration is closer to 0.05 mass fraction. Due to the Zn-contents in the fcc and bcc phases, a maximum limit of 0.35 mass fraction Zn was also established. This condition was also useful in lowering the yellowness of the alloy.

Table 9: Measured compositions (given in mass fractions multiplied by 100) of the bcc and fcc phases present in test alloy C99E-1.

Phase	Ni	Zn	Mn
bcc	4.56 ± 0.08	40.44 ± 0.22	5.02 ± 0.10
fcc	4.95 ± 0.12	35.61 ± 0.19	4.47 ± 0.08

5.2. Monolithic C99 optimization:

5.2.1. Monolithic C99: First prototype

The data collected from the test alloys was used to re-optimize the conductivity model and place restrictions on the alloy composition. A 0.06 mass fraction Ni minimum was set, which was 0.01 mass fraction Ni higher than the measured Ni content in the fcc phase of C99E-1. This composition constraint ensured a fully fcc microstructure for the alloy and allowed for some range in the final composition tolerances. Likewise, as mentioned above, a 0.35 mass fraction Zn maximum was set to avoid the formation of the bcc phase and improve the alloy color.

The measured conductivity of C99G-2 in the A-WQ condition was $5.295 \% \pm 0.023 \%$ IACS, which was slightly lower than the target value (which had not yet been lowered to 5.35% IACS) but reasonable for a first attempt. Additionally, the b^* was 9.45 ± 0.15 , which was below the initial color specification of <10 . Unfortunately, the color of C99G-2 was deemed too yellow upon visual inspection, and thus the US Mint requested a new target b^* of < 7 .

5.2.2. Monolithic C99: Second Prototype

With the new dimension of color introduced into consideration, the first generation color model, Eq. (3), was included as a design constraint. From the model, a $(\text{Ni}+\text{Mn})/\text{Zn}$ ratio ≥ 0.5 was identified as resulting in a b^* of < 7 . The second iteration in the C99 alloy design optimization was performed as follows: 1) two Cu-concentration levels of 0.55 mass fraction and 0.60 mass fraction were chosen, 2) Ni+Mn and Zn concentrations set to have a ratio of ≥ 0.5 , and c) the Ni and Mn content were adjusted to produce an alloy with a calculated conductivity of 5.5% IACS. The compositions were rounded to the nearest whole number percent. Two alloys were identified and produced from these constraints: C99I with a composition of Cu-0.11Ni-0.26Zn-0.03Mn mass fraction (ratio of 0.54 and 60 % Cu), and C99J with a composition of Cu-0.14Ni-0.29Zn-0.03Mn mass fraction (ratio of 0.55 and 54 % Cu). The conductivities of C99I-2 and C99J-1 in the A-WQ condition, again summarized in Table , were $5.640 \% \pm 0.027 \%$ IACS and $5.457 \% \pm 0.007 \%$ IACS, respectively. Both values were within 0.2 % IACS of the target conductivity. The measured b^* values, however, were 7.94 ± 0.41 and 7.35 ± 0.08 for C99I-2 and C99J-1, respectively. Both value were above the new target value of 7.

5.2.3. Monolithic C99: Third Prototype

The second-generation color model was introduced after C99I-2 and C99J-1 were found to be too yellow. The conductivity and color descriptions, along with the acquired knowledge of the fcc/bcc+fcc phase boundary, were then combined in the optimization process to minimize the cost while satisfying all requirements. At this point in the project, enough experimental data had been collected to assess the accuracy of the different models. The conductivity model was found to consistently predict conductivities between 0.1 % IACS and 0.2 % IACS below the experimentally measured values and the color description underestimated b^* by about 0.2. These were taken into consideration, and the optimization process was again performed, this time resulting in the composition (to the nearest 0.5 %) of C99M, Cu-0.135Ni-0.26Zn-0.025Mn mass fraction. Because this composition was so close to that of C99J, it was considered an iterative step from C99J. A composition slightly leaner in Ni was also identified, C99L, Cu-0.11Ni-0.23Zn-0.035Mn mass fraction, which was an iteration of C99I. The measured conductivities of C99L-1 and C99M-1 were satisfactory, being $5.523 \% \pm 0.012 \%$ IACS and $5.447 \% \pm 0.022 \%$ IACS, respectively. However, with b^* values of 8.25 ± 0.28 and 7.38 ± 0.21 for C99L-1 and C99M-1, respectively, the colors were too yellow. In fact, the b^* value actually increased slightly from C99I to C99L and from C99J to C99M despite the measured composition suggesting the change should be in the opposite direction.

5.2.4. Monolithic C99 optimization: Fourth Prototype

Noting that color was not being improved by increasing the Ni content, and that the compositions of C99J and C99M were moving steadily back toward the composition of C77D', it was determined that a b^* of about 7.5 was the best that could be obtained in the quaternary Cu-Ni-Zn-Mn system (and maintain a significant difference in composition compared to C77D'). For these reasons, and the limited remaining resources available for further development, the composition Cu-0.14Ni-0.28Zn-0.03Mn mass fraction, designated C99O, was to be the final alloy in the C99-series monolithic development. When the conductivity of C99O-1 was found to be too low, $5.159\% \pm 0.007\%$ IACS, the final composition was again modified to create C99R, Cu-0.14Ni-0.285Zn-0.025Mn mass fraction. The measured conductivity of C99R-1 was $5.374\% \pm 0.011\%$ IACS. This was determined to be an exceptional match with the amended target value of 5.35% IACS. Heats C99R-2 through C99R-5 were then produced and provided to the US Mint for coining and additional characterization. Coins produced from C99R have been reported to achieve a 100% acceptance rate in three in-house coin acceptor devices at the US Mint. The wear-corrosion results for C99R, summarized in Table 6, are three to four times better than C71300.

5.3. *Characterization and finalization of C99R*

5.3.1. Mechanical properties

Figure 21 compares the tensile behavior of the NIST C99R and NIST C99H cladding alloys to commercial C71300. As was the case with C77D, C99R is stronger and more ductile than the C71300 although the yield strength is nearer to that of C71300. In addition, the initial work hardening properties of C99R are lower than C71300, and even lower the C77D (Table 5). Again this suggests that it may flow more easily during the coin stamping process. The mechanical properties of C99R and C99H are summarized in Table 10.

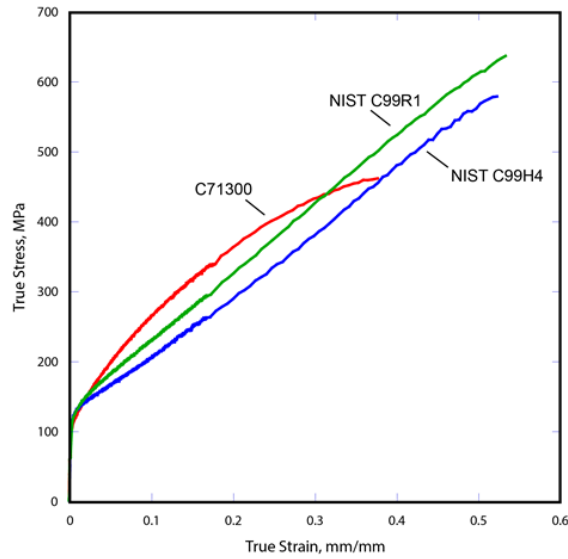


Figure 21: The mechanical properties of NIST C99R and NIST C99R compared to the C71300 commercial binary alloy.

Table 10: Summary of the measured mechanical properties of NIST C99R and NIST C99H compared to C71300. Note: a standard deviation of 0.00 indicates that the actual value is smaller than the range shown in the table.

Alloy	σ_y , MPa	σ_{UTS} , MPa	True Fracture Stress, MPa	Strain to Failure	K (0.01-0.1), MPa	n (0.01-0.1)	K (0.1-0.15), MPa	n (0.1-0.15)
C99R	118 ± 2	373 ± 01	634 ± 30	0.55 ± 0.02	408 ± 10	0.11 ± 0.00	731 ± 24	0.21 ± 0.01
C99H	114 ± 4	347 ± 12	572 ± 24	0.53 ± 0.02	325 ± 09	0.09 ± 0.01	680 ± 09	0.21 ± 0.01

5.3.2. Electrochemical behavior

The performances of C99R and C99H are compared to the C71300 under free corrosion conditions in Figure 22. C99R quickly reached minimum potential, but then it slowly increased over the remainder of the exposure time. It was substantially more cathodic compared to the C71300 binary in the sulfate solution. In the simulated sweat solution, C99R reached a steady-state FCP after approximately 5 hours of exposure time; and again was significantly more cathodic than C71300. No indications of active corrosion (i.e, pits or dealloyed regions) were observed.

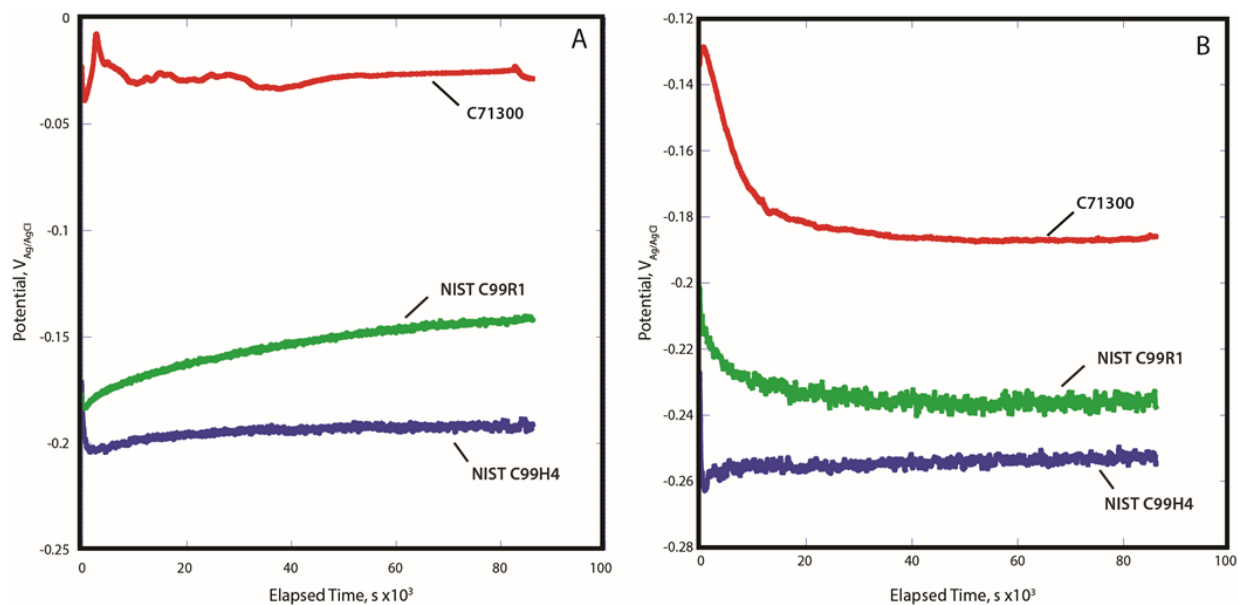


Figure 22: Comparison of alloy performance under free corrosion conditions in a) deaerated 0.5M Na₂SO₄, and b) deaerated simulated human sweat solution.

The polarization resistance of the NIST alloys in the two solutions is compared to the C71300 in Figure 23. As before, the figures are the electrode potential shown as a function of the log of the current. As shown in Figure 23a, the behavior C99R was quite similar to C71300 in the sulfate solution. The behavior of the C71300 binary was slightly more anodic than C99R, but both alloys exhibited a relatively stable region of passivity in the sulfate solution. Like the behaviors C77000 and NIST C77D in Figure 16, the onset of pitting also occurred at approximately 0.000 V wrt Ag/AgCl for C99R.

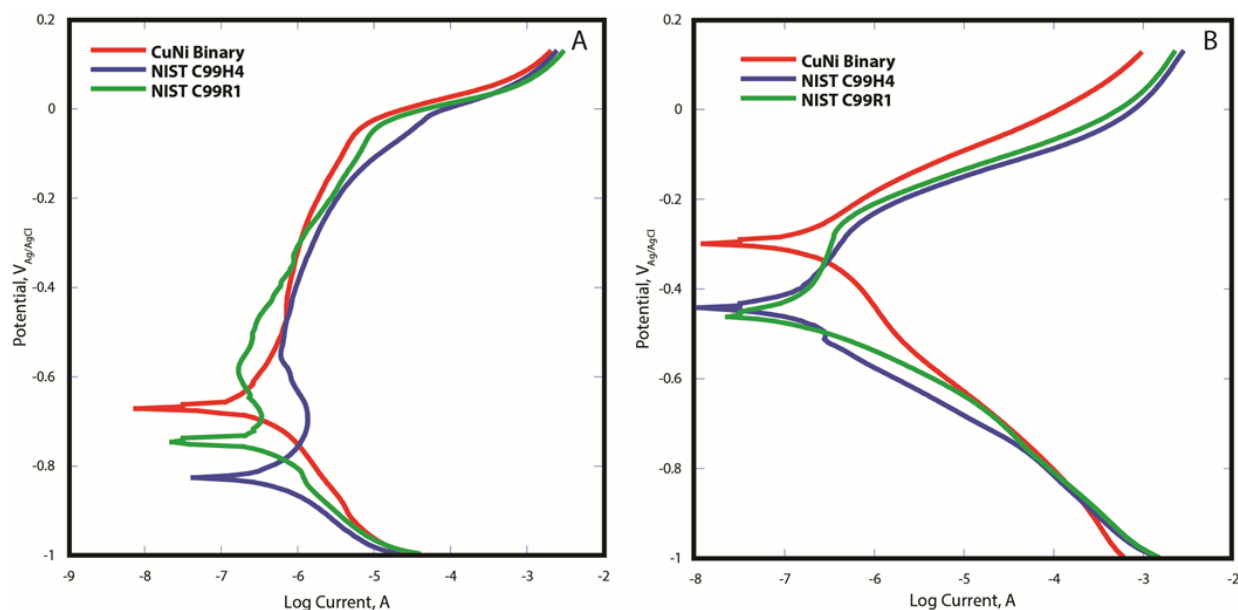


Figure 23: Comparison of C71300, NIST C99R and NIST C99H performance using polarization resistance in a) deaerated 0.5M Na₂SO₄ and b) deaerated simulated human sweat solution.

In the simulated sweat solution (Figure 23*b*), NIST C99R exhibited a short region of passivity in contrast to C71300. Overall, the onset of the anodic region in the simulated human sweat was significantly higher than what was observed in the sulfate. The passive region extended over a larger potential range in the sulfate, but based on these results the performance of C99R should be no worse than C71300 in service.

5.3.3. Composition tolerances

The measured composition and electrical conductivity of C99R-1 (see Table 8) were used to identify appropriate composition tolerances for C99R. Figure 24 shows the composition dependence of conductivity. As with C77D, Zn-content has little effect on conductivity. Thus, the primary concern of the composition tolerances was to ensure extremes in both Ni and Mn did not produce a conductivity outside the ± 0.2 % IACS US Mint requirement. Because resources were not available for experimental investigation of composition limits of C99R, Fe was not directly considered in determining the composition tolerances. Instead, the observed effect of Fe measured in C77F-1 and C77G-1 was used to estimate the tolerance. Fe appears to be about half as effective as Mn in reducing conductivity. The final composition tolerances for C99R are given in the alloy data sheet, Figure 25.

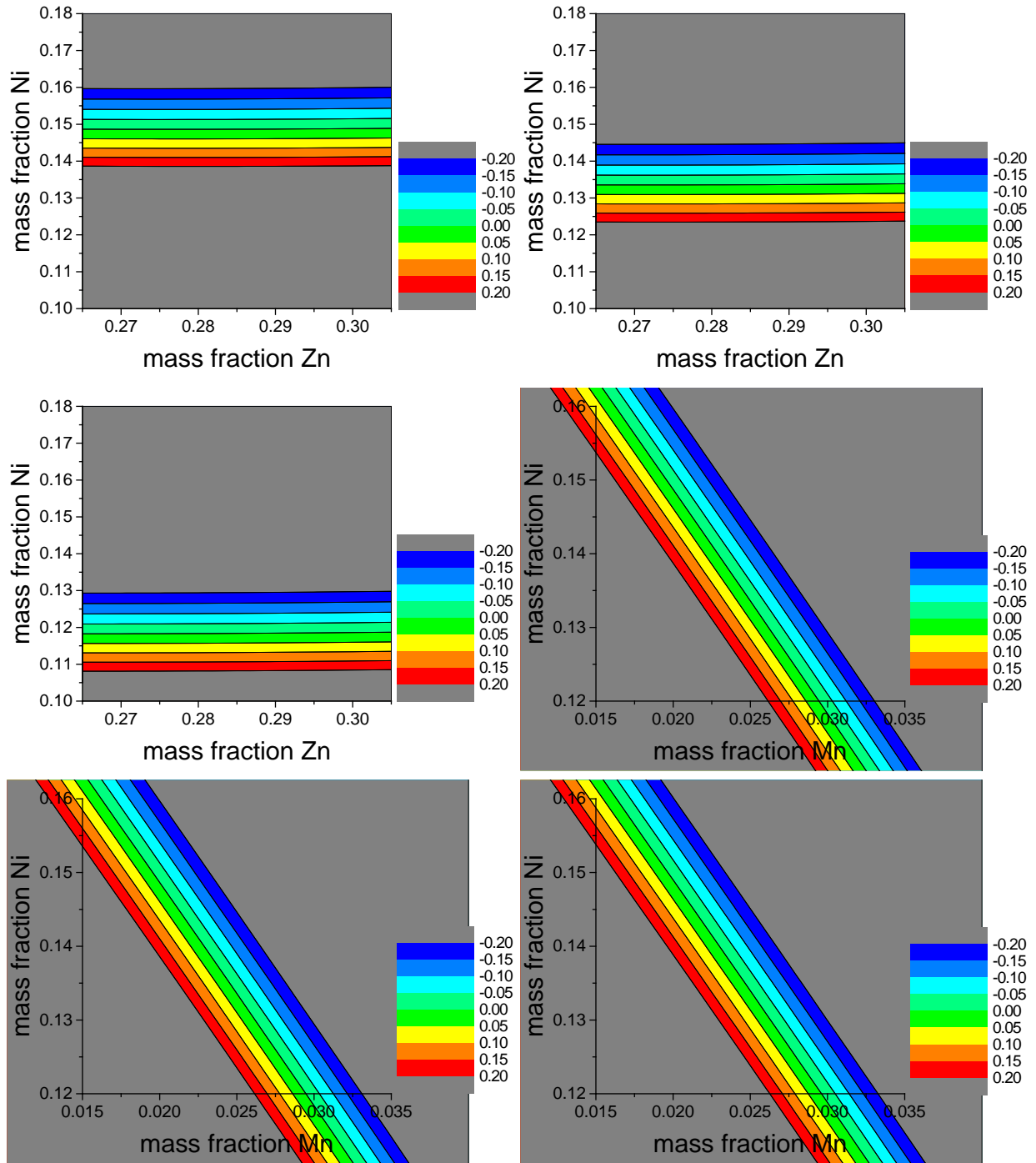


Figure 24: Calculated dependence on composition of the deviation in conductivity (± 0.2 % IACS) from the value calculated for the composition of C77R of 5.13 % IACS in quaternary Cu-Ni-Zn-Mn for Mn compositions of a) 0.02 mass fraction b) 0.025 mass fraction, and c) 0.03 mass fraction, and for Zn compositions of d) 0.26 mass fraction, e) 0.285 mass fraction and f) 0.31 mass fraction.

NIST C99R Alloy Data Sheet

- Composition:

Cu	Ni (14.4 %)	Zn (28.2 %)	Mn (2.2 %)	Fe (0 %)
Bal.	14.0 to 14.7	27.0 to 30.0	2.0 to 2.4	<0.2

- Conductivity (annealed 700 °C to 800 °C, 30 min, water quench): 5.4±0.2 % IACS
- Mechanical Properties (annealed): should be similar to C77D based on hardness data collected from C99O-1 (93 VHN)
- Color: about 7.4, based on data from C99J-1 & C99M-1
- Corrosion: TBD
- Cost: about 25 % less than C71300, based on material costs
- Additional notes:
 - Preliminary tests on C99O-1 indicated little change in conductivity with cooling rate, though the composition similarity to C77000 & C77D suggest ordering may occur in C99R, and thus conductivity may change as a function of cooling rate. However, the alloy was again designed for thermal processing followed by water quenching, and the above properties cannot be guaranteed in other processing conditions are used.

Figure 25: NIST C99R alloy data sheet. All alloy compositions are given in mass fractions multiplied by 100.

5.4. Development of C99 cladding alloy

Because the target conductivity of the C99-series cladding alloy was more flexible, the design was easier than that of C99R. Two of the test alloys, C99B-1 and C99C-1, exhibit properties very close to that desired for the cladding alloy. C99-B was chosen as the first generation C99 cladding alloy, and a 1 kg heat, C99B-2, was produced. However, the color of C99B-2 was much higher than C99B-1, most likely because of the increase in Zn content. This change arose because Zn evaporation was less of an issue in melts of 1 kg, compared to smaller 200 g ingots like C99B-1. Additionally, extra Zn was not included in C99B-1 to offset Zn evaporation. The Zn losses in C99A-1 through C99D-1 were used to determine the correct amount of extra Zn to add.

This change in color from C99B-1 to C99B-2 resulted in a slight modification of the composition, and C99H, Cu-0.06Ni-0.25Zn-0.14Mn mass fraction, was created. C99H-1 had a conductivity of 2.514 % ± 0.009 % IACS and a hardness of (102.6 ± 4.1) VHN100 in the A-WQ state, and a b^* of 5.15 ± 0.10. The hardness was noted as slightly high, though it did not exceed the US Mint specification. The US Mint took the remaining C99H-1 material for further evaluation. They determined during this testing that the surface finish of C99H-1 was insufficient. Thus, both sides of each ingot were milled flat prior to rolling into sheet. Unfortunately, C99H-3 and C99H-4 were cast and rolled prior to this discovery and could not be

used by the US Mint. Therefore, portions of these two heats were used for NIST mechanical and corrosion testing.

Heats C99H-5 and C99H-6 were the first pair of C99H samples to be processed with a milled surface. The alloys were also rolled into a single sheet that was between 50 cm to 60 cm in length, and then sent to a third-party company performing the cladding process. The conductivities of C99H-5 and C99H-6 were $2.683 \% \pm 0.007 \%$ and $2.689 \% \pm 0.023 \%$, respectively. The slight increase in conductivity compared to C99H-1 was due to a decrease in Mn-content, which was lost during melting. It was known prior to melting the C99H alloys that Mn loss due to evaporation would be an issue similar to the Zn evaporation. However, when melting C99H alloys in practice the control of the Mn loss was found to be more difficult to control because Mn reacted with the crucible and formed a slag on the surface of the melt. This slag made it difficult to determine whether the pure elements were completely melted. The Mn-loss per heat varied as function of the time melt was superheated and stirred (see Table 8 for the Mn-content of all C99H heats produced).

Despite the slight variation in Mn content, C99H-5 and C99H-6 were sent to the US Mint for cladding and testing. Unfortunately, the third-party company made an error during the cladding process and the thickness ratios were not correct. Two additional C99H melts, C99H-8 and C99H-9, had to be produced and were provided to the US Mint for cladding and testing purposes. These heats had compositions closer to that of C99H-1, suggesting their conductivities were likely less than those of C99H-3 through C99H-6. At the time of preparation of this report these characterization experiments were ongoing at the US Mint.

5.5. Characterization and finalization of C99H

5.5.1. Mechanical behavior

The strength of C99H was expected to be higher than the binary or ternary alloys due to an increase in solid solution strengthening via large Mn additions. In practice, however, the opposite was observed. As shown in Figure 21, C99H-4 is not as strong as the C99R. It has similar ductility to the C99R, but it also has a lower initial work hardening rate. Both the C99H and the C99R are stronger and more ductile than the C71300. The mechanical properties of C99H are summarized in Table 10, along with those of C99R. Note the composition of the material used for mechanical and corrosion testing is lower in Mn. If the Mn-content was increased approximately 1.5 percent, the strength would likely increase. Using the available microhardness and tensile data (i.e., a yield strength of 40 percent of the ultimate tensile strength of commercial C77000, and a 10 percent underestimate in the ultimate tensile strength predicted from hardness data for C99H-3), the maximum yield stress that could be expected for an alloy with a Mn-content of 14 % would be about 150 MPa, which would be well below the US Mint specification.

The reason for the decreased strength in C99H is not entirely clear. One possible explanation can be found in the microstructure of C99H in the A-WQ state (Figure 26). The grain size of C99H-3 annealed for 30 min at 775 °C followed by water quenching is on the order of 300 μm or

larger as compared to that of C77M-1 (Figure 9), which are only 100 μm to 200 μm even after annealing for 30 min at 850 $^{\circ}\text{C}$. During commercial production, tramp impurity elements such as Fe, Pb, etc., will most likely act as grain refiners and slow grain growth. This could produce a stronger material, although it is unlikely that the mechanical properties will exceed those specified by the US Mint. Tests during up-scaling will be required for confirmation.

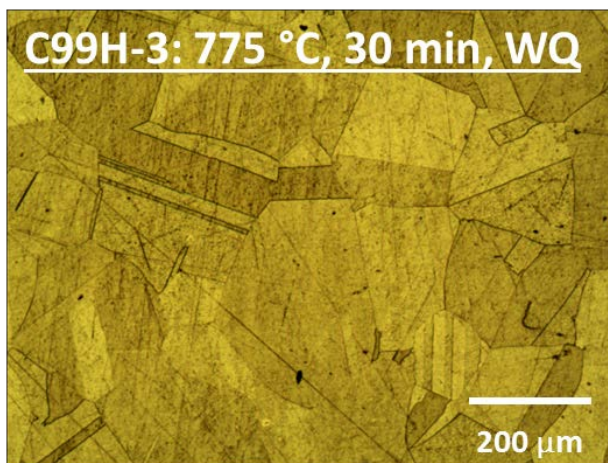


Figure 26: Microstructure of C99H-3 annealed at 775 $^{\circ}\text{C}$ for 30 min, then water quenched.

5.5.2. Electrochemical behavior

Of the three curves shown in Figure 22, C99H appears to be the most stable in the sulfate solution. This alloy reached a steady-state potential within a few hours, and then maintained that potential for the remainder of the exposure time. As was the case with C99R, C99H was substantially more cathodic than C71300 in the sulfate solution. C99H also exhibited a similar trend in the simulated sweat solution. No indications of active corrosion were observed on the surface of the C99H sample.

As shown in Figure 23a, the behavior of the C99H was quite similar to C99R and C71300 in the sulfate solution. All three alloys exhibited a relatively stable region of passivity in the sulfate solution. The onset of pitting occurred at approximately 0.000 V wrt Ag/AgCl. In the simulated sweat solution, the behavior of C99H was fairly similar to those exhibited by C99R and C71300. The one difference was C99H exhibited a short region of passivity similar to C99R, which was not observed for C71300. Based on these results, the performance of the C99H is expected to be similar to the C71300 in service.

5.5.3. Composition tolerances

Due to the lack of a well-defined target conductivity for the C99 cladding alloy, and to the variation in Mn-content (which produced variability in the conductivity between C99H heats), defining composition tolerances for the C99H alloy proved more difficult than for the other two prototype alloys. Therefore, three sets of composition tolerances have been defined based on the

following: a) the $\pm 0.2\%$ IACS specification of the US Mint surrounding three central target conductivities, b) the 2.6% IACS (the calculated conductivity for C99H-1, likely that of C99H-8 and C99H-9), c) the 2.8% IACS calculated conductivity of C99H-3, and d) the average of 2.7% IACS.

Figure 27 plots the effect Ni and Zn composition on the deviation in conductivity from 2.7% IACS, and demonstrates that the Zn-content plays a larger role on conductivity than for C77D or C99R. That is, the isolines on the plots are not parallel to the Zn-axis. However the range in Ni-content over which the conductivity remains within the $\pm 0.2\%$ IACS requirement has increased. This suggests that the Ni-content has less of an effect on conductivity with the increased Mn-content. Figure 28 illustrates this relationship as it shows absolute conductivity as a function of Mn- and Ni-content for constant Zn mass fractions of 0.21, 0.25, and 0.29. In contrast to those in Figure 24, the isolines in this figure are almost parallel to the Zn axis; and this trend continues to lower Mn-content as shown in Figure 17.

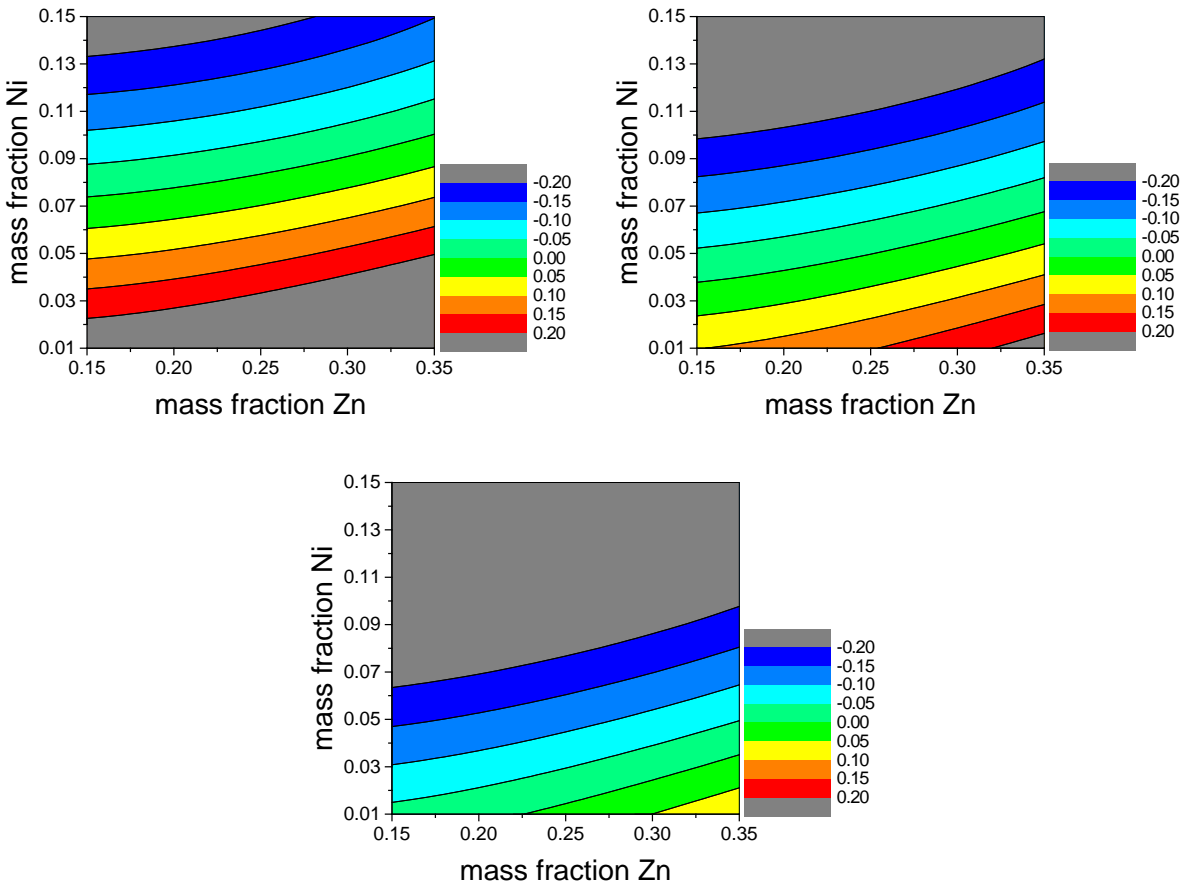


Figure 27: Dependence of Ni- and Zn-content on the deviation in calculated conductivity from 2.7% IACS in C99H alloys for constant mass fractions of Mn of a) 0.13, b) 0.14, and c) 0.15

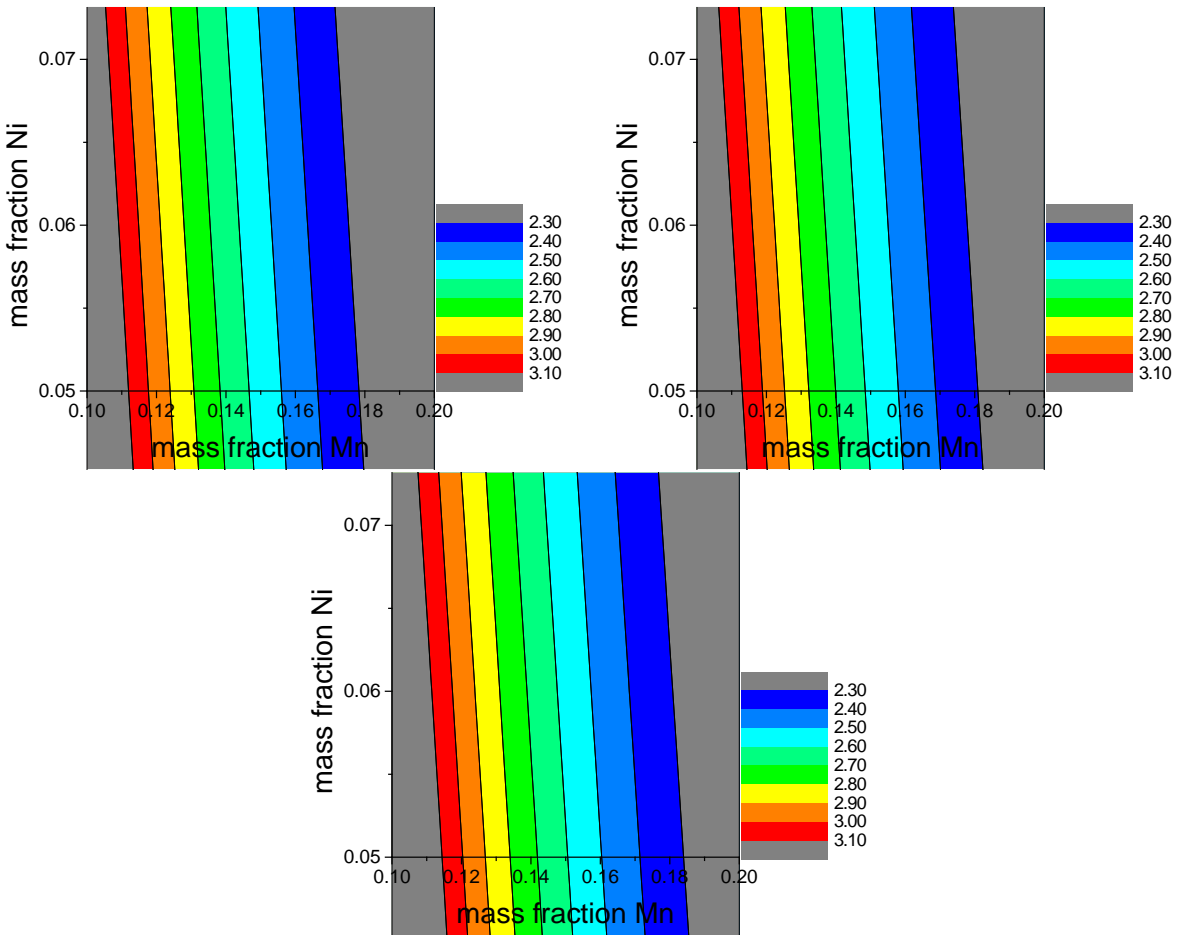


Figure 28: Dependence of Ni- and Zn-content on the calculated absolute conductivity for constant mass fractions of Zn of a) 0.21, b) 0.25, and c) 0.29.

Because of the smaller effect on Ni and Zn on conductivity and the smaller variation in measured composition between C99H heats, the composition limits for these two elements were the same for all three tolerance limits. The composition limits for Zn are between 0.23 mass fraction and 0.27 mass fraction, and for Ni the limits are between 0.055 mass fraction and 0.065 mass fraction. From Figure 28, the composition limits for Mn were $\pm 1\%$ Mn mass fraction surrounding mass fractions of 0.145, 0.14, and 0.13 for target conductivities of 2.6 % IACS, 2.7 % IACS, and 2.8 % IACS, respectively. Figure 29 is the data sheet for C99H, providing all relevant properties, including the potential variation of alloys with different target conductivities.

6. Conclusions/Summary

NIST employed a materials design approach centered on CALPHAD-based models to develop three new coinage materials for the US Mint to assuage the production cost of US coinage. Two monolithic prototypes and one cladding prototype were designed using CALPHAD-base models for the thermodynamics, kinetics, electrical conductivity, and color. The computationally

designed prototypes were produced and characterized in the NIST laboratories using processes as similar as possible to the actual manufacturing processes used by the US Mint.

All three prototype alloys are ready to be provided to US Mint material suppliers for up-scaling to commercial production levels. Clearly, some processing issues could arise during the transition to industrial levels that are not observed at the laboratory scale (such as impurity concentrations in industrial quantities that are greater than those at the laboratory scale) and the computational design models should help address some of these issues. The patent protection process for each alloy is in progress and non-disclosure agreements are in place with two US Mint materials suppliers.

The CALPHAD-based thermodynamic assessments were used to determine composition regions that would produce a single-phase fcc region within the US Mint processing conditions. The equilibrium fcc/bcc phase boundary data acquired can be used to refine the current Cu-Ni-Zn-Mn thermodynamic assessments. The CALPHAD-based electrical conductivity model for the fcc Cu-Ni-Mn-Zn system successfully predicted the conductivity properties of the prototypes. This is the first application of phase-based conductivity model include in materials design process and will serve as model for other materials design applications.

The electrochemical analysis indicated that Zn dealloying could occur if the passivating film was breached. This dealloying could then potentially reduce the corrosion resistance of the coin. While initial results indicated the current US Mint passivation process is compatible with the new prototypes, additional testing may be needed to verify this result. The electrochemical results provided a new baseline by which more quantitative corrosion analysis can be considered for future coinage materials. The current steam testing performed by the US Mint is highly dependent on the measurements conditions for the alloy color before and after exposure to the steam environment.

The new cladding alloy met all the required US Mint specifications. However the US Mint did not specify the processing that would be to use to bond the cladding material to the core material. It is anticipated that this process will proceed smoothly as both the cladding and core materials are comprised of the same alloying elements, but there is the potential for diffusion between the two materials that may cause the formation of unwanted phases. Using multicomponent multiphase diffusion simulations bonding conditions could be recommended to avoid potential unwanted phases.

The success of this materials design approach should serve as an example for future materials design applications. The thermodynamic, electrical conductivity, color, and cost models can all be used for other applications and expanded to new alloys systems.

NIST C99H Alloy Data Sheet

- Composition:

Target conductivity	Cu	Ni (6 %)	Zn (25 %)	Mn (13-14.5 %)	Fe (0 %)
2.6 % IACS	Bal.	5.5 to 6.5	23.0 to 27.0	13.5 to 15.5 (14.5)	<0.2
2.7 % IACS	Bal.	5.5 to 6.5	23.0 to 27.0	13.0 to 15.0 (14)	
2.8 % IACS	Bal.	5.5 to 6.5	23.0 to 27.0	12.0 to 14.0 (13)	

- Depending on the target conductivity above, after being annealed at 700 °C to 800 °C for 30 min and water quenched, the conductivity will be the stated value ± 0.2 % IACS
- Mechanical Properties (annealed):
 - Yield strength: 115 \pm 20 MPa (2.8 % IACS) up to 150 \pm 20 MPa (2.6 % IACS)
 - Strain to failure: >50 %
 - Work-hardening exponent: 0.1 ($\epsilon=0.01$ to 0.1), 0.2 ($\epsilon=0.1$ to 0.15)
 - TBD
- Corrosion: TBD
- Cost: about 35 % less than C71300, based on material costs
- Additional notes:
 - The composition of the alloy should be outside of the range in which it would undergo atomic-level ordering thus making conductivity and mechanical behavior a function of cooling rate. However, the alloy was designed for thermal processing followed by water quenching, and the above properties cannot be guaranteed in other processing conditions are used.

Figure 29: NIST C99H alloy data sheet. Al compositions are given mass fraction multiplied by 100.

Appendix A: More cost-effective C99-series alternatives and the issue of color

As mentioned in section 5.2.1, the first alloy designed using the combine models, C99G, possessed an electrical conductivity very near that required for the replacement of C71300. Unfortunately, the color was deemed too yellow. In addition to the alloys described in section 5, Table also includes a number of other alloys; most of which with much leaner Ni-content compared to C77D or C99R, and thus less expensive. The measured compositions, electrical conductivities, b^* yellowness values, and relative material cost compared to C71300 of these alloys are summarized in Table 11.

Table 11: Measured compositions, conductivities, and b^ values, and cost savings versus C71300 for several “side-project” alloys designed to meet the required conductivity requirement, but which fell short in terms of color. Also shown are C71300, C77D, and C99R-1. ^aC99E-2 contained a small fraction of a second phase (bcc) and was never considered further; although the conductivity and color suggests it could be developed further to be single phase fcc, though C99G-2 and C99N-1 have similar Ni- and Mn-contents but less Zn and were single-phase fcc but colors deemed too yellow.*

Alloy	Measured Composition (by mass fraction x100)	Conductivity, % IACS (480 kHz)	b^*	Cost savings vs C71300
C71300	Cu-25.8Ni-0.3Mn	5.35 ± 0.06	5.61 ± 0.28	-
C77D (all)	Cu-19.3Ni-26.2Zn-0.3Mn	5.40 ± 0.09	5.54 ± 0.03	20 %
C99R-1	Cu-14.4Ni-28.2Zn-2.2Mn	5.37 ± 0.01	N/A	26 %
C99E-2 ^a	Cu-4.6Ni-35.0Zn-5.1Mn	5.25 ± 0.03	6.65 ± 0.37	39 %
C99G-2	Cu-7.5Ni-30.9Zn-4.6Mn	5.26 ± 0.02	9.45 ± 0.15	34 %
C99K-1	Cu-9.5Ni-28.7Zn-3.4Mn	5.64 ± 0.01	9.10 ± 0.28	30 %
C99N-1	Cu-5.2Ni-20.3Zn-5.4Mn	5.47 ± 0.02	10.24 ± 0.21	30 %
C99P-1	Cu-8.0Ni-22.5Zn-4.6Mn	5.34 ± 0.01	9.99 ± 0.34	29 %
C99Q-1	Cu-10.6Ni-24.0Zn-3.9Mn	5.34 ± 0.01	8.97 ± 0.55	27 %

Each of the six additional alloys listed in Table 1, beginning with C99E-2, may offer significant cost savings over C71300 and the two NIST-designed alloys developed in this project. The conductivities are all within about 0.2 % IACS of the US Mint requirement, and could be made a match with slight modifications to composition. As mentioned, with the exception of C99E-2, the issue with all of these alloys is the measured color. In the case of C99E-2, the issue was not color, but the presence of a second phase, bcc, in the alloy microstructure. This too may be solved by a small change in composition. In fact, C99G was designed as an iteration of C99E-2, with more Ni to create a single-phase fcc microstructure and less Zn to improve the color. The microstructure was indeed single-phase, but surprisingly the measured color actually increased by nearly 50 %.

The color measurements for several other alloys were quite surprising, considering the observed trends in yellowness with composition. For instance, moving from C99J-1 to C99M-1 (see Table) had almost no change in b^* , despite a decrease in Zn-content by 0.03 mass fraction while the Mn and Ni concentrations remains nearly the same. Moreover, b^* actually increased from C99I-2 to C99L-1, where again the Zn-content was decreased by 0.03 mass fraction, the Ni-content

remained constant, and the Mn level increased by 0.005 mass fraction. It was also noted that in many cases the difference in color between these alloys and C71300 or C77D was indistinguishable to the unaided eye.

Much of this scatter may be attributed again to the highly inexact nature of measuring alloy color. C99B-2, for instance, exhibited five different b^* values in five separate instances. In the as-rolled condition, after being polished with 400 grit grinding paper, the b^* value was 6.95. After annealing and re-polishing with 400 grit grinding paper, b^* value was 13.86. Polishing the same sample again resulted in a value of 10.34; and after waiting four hours, the re-measured surface had b^* value of 12.07.

The lack of quantitative color measurement was a significant issue in the development of the C99-series monolithic alloy. Unfortunately, the scope of the project and available resources were insufficient to investigate potential further development of the alloys listed in Table 11. If a more quantitative color measurement could be developed, an improved color model could be constructed and be used to design even lower cost coinage materials that still meet the US Mint requirements conductivity, color, mechanical properties, corrosion and wear resistance and processing conditions.

Acknowledgements

Funding for this work was provided by the Interagency Agreement between the US Mint and the National Institute of Standards and Technology, HQ14RA-38 NISTMOD. 001 (IA# 1404-642-01). The authors would also like to thank Sandy Claggett of the NIST MSED for her valuable assistance with the metallography of these alloys and Kil-Won Moon and Richard Ricker of NIST for the valuable feedback.

References

1. Stossel RJ, Tims ML, Pickens JR, McNamara DK, McCann MG, Decker RF, Alternative Metal Study. Concurrent Technologies Corporation submitted to the US Mint , August 31, 2012.
2. ASM Alloy Phase Diagram Database (2015) ASM International.
<http://www1.asminternational.org/asmenterprise/apd/>.
3. Jiang M, Wang CP, Liu XJ, Ohnuma I, Kainuma R, Vassilev GP, Ishida K, Thermodynamic calculation of phase equilibria in the Cu-Ni-Zn System. *J. Physics & Chem. Solids* 66 (2005) 246-250.
4. Miettinen J, Thermodynamic description of the Cu-Ni-Zn system above 600 C. *CALPHAD* 27 (2003) 263-274.
5. Miettinen J., Thermodynamic description of the Cu-Mn-Ni system at the Cu-Ni side. *CALPHAD* 27 (2003) 147-152. doi:10.1016/j.calphad.2003.08.003.
6. Miettinen J, Thermodynamic description of the Cu-Mn-Zn system in the copper-rich corner. *CALPHAD* 28 (2004):313-320. doi:10.1016/j.calphad.2004.09.003.
7. Campbell CE, Kattner UR, Liu ZK , The development of phase-based property data using the CALPHAD method and infrastructure needs. *Integrating Materials and Manufacturing Innovation* (2014) 3:23. doi:doi:10.1186/2193-9772-3-12.
8. Nordheim L, Electron theory of metals I. *Ann Phys-Berlin* 9 (1931) 607-640.
9. Schroder K *CRC Handbook of Electrical Resistivities of Binary Metallic Alloys*. CRC Press, Boca Raton, Florida, 1983.
10. Copper Development Association, <http://www.copper.org/>. Accessed November 2014
11. AlB Copper Alloys Company Ltd. <http://www.alb-copperalloys.com/>. Accessed November 2014
12. Substances and Technologies. <http://www.substech.com/>. Accessed November 2014
13. J.E. Brookes Metals. <http://www.ejbmets.com/>. Accessed November 2014
14. Lahiri A, Mukherjee K, Banerjee T Studies on the properties of some copper-manganese alloys. In: Symposium on Metallurgy of Substitute Ferrous & Non-Ferrous Alloys, Jamshedpur, India, April 27-30, 1966. NML,
15. Zhang YP, Zhang JX, Wu JS, Quantitative research on color of Cu-Mn-Zn alloys. *Mater Trans* 43 (2002):741-744. doi:10.2320/matertrans.43.741